Tree Height Estimation Using Field Measurement and Low-Cost Unmanned Aerial
Vehicle (UAV) at Phnom Kulen National Park of Cambodia

LY MOT

A THESIS SUBMITTED IN PARTIAL FULFILLMENT OF

THE REQUIREMENTS FOR THE MASTER DEGREE OF SCIENCE

IN GEOINFORMATICS

FACULTY OF GEOINFORMATICS

BURAPHA UNIVERSITY

2021

การประมาณความสูงของต้นไม้โดยใช้การวัดภาคสนามและ อากาศยานไร้คนขับต้นทุนต่ำ (UAV) ที่อุทยานแห่งชาติพนมกุเลนของกัมพูชา

LY MOT

วิทยานิพนธ์นี้เป็นส่วนหนึ่งของการศึกษาตามหลักสูตรวิทยาศาสตร
มหาบัณฑิต
สาขาวิชาภูมิสารสนเทศศาสตร์
คณะภูมิสารสนเทศศาสตร์ มหาวิทยาลัยบูรพา
2564

Tree Height Estimation Using Field Measurement and Low-Cost Unmanned Aerial
Vehicle (UAV) at Phnom Kulen National Park of Cambodia

LY MOT

A THESIS SUBMITTED IN PARTIAL FULFILLMENT OF
THE REQUIREMENTS FOR THE MASTER DEGREE OF SCIENCE
IN GEOINFORMATICS
FACULTY OF GEOINFORMATICS
BURAPHA UNIVERSITY
2021

The Thesis of Ly Mot has been approved by the examining committee to be partial fulfillment of the requirements for the Master Degree of Science in Geoinformatics of Burapha University

Advisory Committee   Examining Committee

Principal advisor

.... Principal examiner
(Professor Hong Shu)   (Assistant Professor Hui Li)

.... Member
Co-advisor   (Professor Hong Shu)

.... Member
(Doctor Kitsanai Charoenjit)   (Professor Timo Balz)

.... Member
(Doctor Haoran Zhang)   (Doctor Kitsanai Charoenjit)

.... External Member
(Doctor Pramet Kaewmesri)

.... Dean of the Faculty of Geoinformatics
(Doctor Kitsanai Charoenjit)
....

This Thesis has been approved by Graduate School Burapha University to be partial fulfillment of the requirements for the Master Degree of Science in Geoinformatics of Burapha University

.... Dean of Graduate School
(Associate Professor Dr. Nujjaree Chaimongkol)
....

62910209:　　　MAJOR: GEOINFORMATICS; M.Sc. (GEOINFORMATICS)

KEYWORDS:　Tree Height, Canopy Height Model, Digital Terrain Model, Digital Surface Model

LY MOT : TREE HEIGHT ESTIMATION USING FIELD MEASUREMENT AND LOW-COST UNMANNED AERIAL VEHICLE (UAV) AT PHNOM KULEN NATIONAL PARK OF CAMBODIA . ADVISORY COMMITTEE: HONG SHU, , KITSANAI CHAROENJIT HAORAN ZHANG 2021.

Tree height estimation is one of the most important parameters used to quantify timber resources. Among others it is used to evaluate the ecological and economic value of forest stand, to calculate the individual and number of stand volumes, and to estimate the forest inventory. In order to update information about forests. This helps local, regional, or national authorities to take decisions and manage the forest.

Most tree estimations with Light Detection and Ranging (LiDAR) have been used successfully over the recent decades. In contrast to LiDAR, estimation of tree height derived Canopy height model (CHM) has been applied with low-cost UAV with acceptable accuracy which is used onboard GPS to obtain a high accuracy of CHM.

This research aims to estimate, and evaluate tree height from high resolution images of low-cost UAVs. The influence of different flight attributes, point cloud densities, extraction methods, photogrammetry products, and point cloud classification are discussed. The estimation of tree height was performed by two extraction methods, photogrammetry product, and point cloud classification. Each was divided into five groups: CHM from the point could classifications, CHM from photogrammetry products-customized with georeferenced methods, CHM from photogrammetry products-defaults with georeferenced methods, CHM from photogrammetry products-defaults without georeferenced methods, and CHM from photogrammetry products- customized without georeferenced methods. Tree heights were obtained from the field with buffering distances of 0 cm, 50 cm, 100 cm, 150 cm, and 200 cm. In total 50 measurements were taken and analyzed in the present study.

First, the results of tree height extraction were successfully taken from UAV data and point cloud classification. In contrast, photogrammetry products produced tree height estimation with extreme bias. In addition, high point cloud densities from 50 m flights provided good data to remove point cloud outliers. The highest R^2 was 0.60. During 200 m flights, R^2 of 0.50 was the highest. Additionally, sample paired t-test, tree height estimation, and ground data from 50 m flight were not statistically significant different.

In sum, this proposed method is possible for open terrains less than 12 m. It is limited by the design of the pipe meters as the measurement of height and cashew leaves was challenging. Regarding the performances of tree height estimation from UAV and field measured, we proved that the workflow of UAV is faster and more effective than field measured which required less times and resources.

ACKNOWLEDGEMENTS

TABLE OF CONTENTS

Page

LIST OF TABLES

Page

LIST OF FIGURES

Page

LIST OF ACRONYMS AND ABBREVIATIONS

DTM : Digital Terrain Model

DSM : Digital Surface Model

CHM : Canopy Height Model

LiDAR : Light Detection and Ranging

UAV : Unmanned Aerial Vehicle

RTK : Real Time Kinematic

GPS : Global Positioning Sytem

3D : Three Dimensional

DGPs : Differential GPS

AGL : Above Ground Level

GCPs : Ground Control Points

m : Meter

cm : Centimeter

CHAPTER 1
INTRODUCTION

1.1 Statements and Significance of the Problems

Tree height is one of the most important sources used to quantify timber resources. It is used to evaluate the ecological and economic value of forest stand. It has been used to compute the individual and number of stand volumes(S. Krause, T. G. M. Sanders, J.-P. Mund, & K. Greve, 2019b). Tree height plays an important role in the regeneration rate of forests and its pattern. It provides habitats for animals (M. F. Ramli & K. N. Tahar, 2020) and production to humans (Phalla et al., 2018). In its inventory, accurate information as the height of the tree and diameter at breast height (DBH) of tree height are very useful. The quantification of the DBH and tree height are possible to measure at the field (Moe, Owari, Furuya, & Hiroshima, 2020). However, field measurements of tree heights are difficult to derive high accuracy because of tall and dense canopies, and crowns (Larjavaara & Muller-Landau, 2013; Sibona et al., 2017). In addition, height measurement using laser range finder (forestry standard method), required times for observing the individual tree and limited for the large area (Zainuddin, Jaffri, Zainal, Ghazali, & Samad, 2016).

The development of new technologies in Remote Sensing (RS), has been used in various applications in forest investigation such as growth, quality prediction, and refined management. Satellite images can be used to determine forest parameters with high precision using an inversion regression model on a large scale. An application on individual trees is not suitable because the spatial resolution is in the range of several meters. In addition, weather conditions and dates for download can affect the accuracy of canopy height estimation (He, Yan, Chen, & Cheng, 2019). Two commonly used remote sensing techniques are airborne laser scanning (ALS) and digital aerial photogrammetry (Moe et al., 2020). Over the recent decades, the active remote sensing technique of ALS, uses light detection and ranging (LiDAR) sensors are possible to measure tree height from three-dimensional (3D) of vegetation canopy components. It includes sub-canopy topography which provides high accuracy of tree height and ground elevation comparable with field measurement (Ganz, Käber, & Adler, 2019; Krause et al., 2019b; Singh et al., 2018; Singh, Evans, Tan, & Nin, 2015). However,

the limitation of LiDAR data acquisition is expensive, which is challenging for forest management authorizes to access the data (He et al., 2019; Krause et al., 2019b; Moe et al., 2020).

The development of unmanned aerial vehicle (UAV) with a consumer-grade onboard camera allowed its to obtain high resolution image for a reasonable price, which provides a large new field of opportunities. Among others, these vehicles can be applied for estimating height with respect to ground surface. Canopy Height Model (CHM), high-resolution DTM, and photogrammetric point clouds are used to estimate individual tree heights (He et al., 2019). Low-cost UAV camera has been applied in various types of terrain to estimate tree heights (Zarco-Tejada, Díaz Varela, Angileri, & Loudjani, 2014). The applied UAV contained a consumer-grade RGB camera and a fixed-wing with 2 m wing span to collect data from 158 ha. The quantification of tree height was derived from high-resolution DSM and orthomosaic from Pix4D software. The estimation of crop height was done by close flight to object in order to improve the spatial resolution(Anthony, Elbaum, Lorenz, & Detweiler, 2014). Wider coverage fisheye lens sensor which is possible to create 3D terrain modelling and Phantom 2 Vision UAV with FC200 wide angle lens camera which provides better accuracy compared to other fisheye lens (Zainuddin et al., 2016). In addition, low-cost UAVs are reliable to apply for estimating various canopy heights and its crowns such as Pinus Pinea plantation (Guerra et al., 2016), Pine tree (A. C. Birdal, Avdan, & Türk, 2017), Pinaceae and Taxodiaceae (Lim Ye et al., 2015), and Olive tree(Díaz-Varela, De la Rosa, León, & Zarco-Tejada, 2015). Low-cost UAV has been successfully applied to estimate tree height using SfM approach. Two methods commonly used for estimating tree height from SfM such as point cloud classify to derived CHM (Ganz et al., 2019; He et al., 2019; Jurjević, Liang, Gašparović, & Balenović, 2020; Wu, Johansen, Phinn, Robson, & Tu, 2020; Zainuddin et al., 2016) and photogrammetry software to generate CHM (Lim Ye et al., 2015; Panagiotidis, Abdollahnejad, Surovy, & Chiteculo, 2017; Zarco-Tejada et al., 2014). Tree height estimation using UAVs have to be considered the ground surface due to the UAV tree height provides average 0.4 m in height precision (Zainuddin et al., 2016). Tree height from UAV refers to the distance between ground to top of canopy which both point cloud classification and photogrammetry software are able to produce DTM and DSM. Different flight attribute produces

different Ground Sampling Distance (GSD). Islami et al. (2021) estimated canopy cover using UAV. They performed three flights by the altitudes of 80 m, 100 m and 120 m with overlaps of 80 % and side overlaps of 70 %. The flight in 100 m provided the best results. Kameyama and Sugiura (2020) proposed different flight attributes, overlap and side overlap to verify tree estimation: altitudes of 60 m, 80 m, 100 m, 120 m, 140 m, overlaps of 80%, 85%, 90%, and 95% and side overlaps of 80%, 85%, 90%, and 95%. The tree height estimation was lower than the actual height. Peng, Zhao, Chen, Chen, and Liu (2021) proposed different point cloud densities such as 12, 17, 28, 64, and 108 points/m^2 with coniferous forest, broad-leaved forest, and mixed coniferous and broad-leaved forest. Tree height extraction from 12 points/m^2 provides greater accuracy compared to other point cloud densities. Thus, UAV tree height estimation should consider method uses such as photogrammetry software products, point cloud density, interpolation methods, and feature extraction.

DJI Phantom 4 series has been successfully applied for estimating tree height. New version of DJI Phantom 4 real-time kinematics (RTK) provides direct geo-referencing with accuracy of a few centimeters (Taddia, Stecchi, & Pellegrinelli, 2020). Moreover, it is also less GCPs needed.

Tree Height measurement obtains the vertical distance between the ground and the top of a tree. It provides useful information in the field of forest research. The accuracy, the time consumption, usage of resources, and common methods have been discussed. Canopy Height Model (CHM) represents tree height from 3D point cloud classifications between the top of canopy (Digital Surface Model-DSM) and bare ground (Digital Terrain Model-DTM). The most frequently method used to estimate tree height is airborne laser scanning, which provides very accurate 3D reconstruction of trees and forests. However, the cost is high compared to passive optical sensors. The accuracy of tree height estimation using low-cost unmanned aerial vehicle (UAV) from difference point cloud densities, flight attributes, overlapping, and type trees have been analyzed. This study focuses on estimating, comparing, and evaluating tree height by photogrammetric point clouds and UAV software, supported by fieldwork to increase the accuracy.

1.2 Research Questions

- Considering different flight attributes, is there any difference in height estimation upon the altitude?
- How to choose the correct flight attribute for tree height estimation?
- How does the accuracy of photogrammetry products perform in tree height estimation?
- Extraction tree height from Canopy Height Model (CHM), which extraction methods (none-buffering and buffering) provide better accuracy?
- How does the accuracy of field measurement validate the tree estimated?

1.3 Research Objective

1. To extract tree height using very high resolution images from low-cost UAV
2. To assess the individual tree height estimation with field measurement

1.4 Conceptual Framework

This research would like to experiment on tree height extraction and analysis on the experimental results from UAV Images. Digital Terrain Model and Digital Surface Model were the main parameters used to identify the height of a tree. Conceptual framework of this research show in Figure 1.
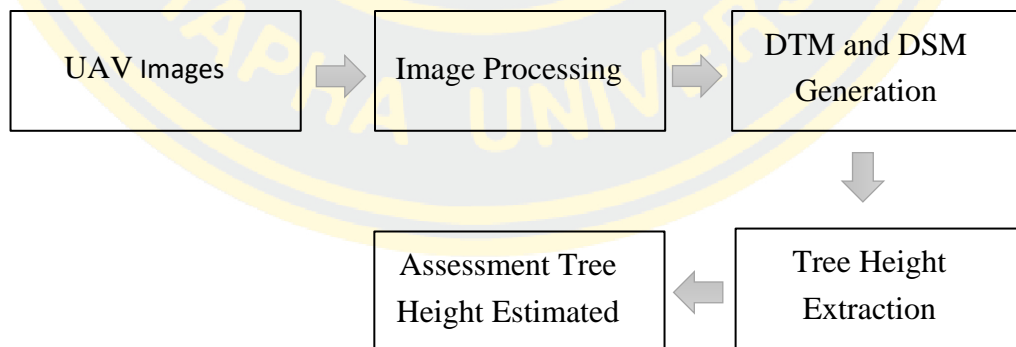
Figures 1 Conceptual Framework of Tree height Estimation in This Research

1.5 Contributions to the Knowledge

The research direction of this study is producing the appropriate method to generate tree height from UAV images. The experimental and analysis on the results of tree height extraction are the useful information and reference use for further study in

the tree height estimation. The methodology of this study is informative concepts for decreasing the field measurement and time consumption in tree height research. This study also possible to use with similar plantations and provides the acceptable result compare to ground data.

CHAPTER 2
LITERATURE REVIEW

2.1 Overview of Photogrammetry

Triangulation technology is the basic principle used in photogrammetry. The line of sight is capturing pictures from at least two different locations then it is generated from each camera to a point on the object. The line of sight is sometimes called a ray because of its optical nature. It can be used mathematically to generate 3D coordinates of the point. Triangulation is the basis that theodolite has used to measure coordinates. It is similar to the two human eyes which work together to measure distances, depth perception (Awange & Kiema, 2019). Photogrammetry was a relatively old discipline historically, with the word "photogrammetry" being coined by Meydenbauer in 1893. The early stages of photogrammetry creation focused primarily on terrestrial surveys, but inaccessible objects such as mountains, expeditions, glaciers, and buildings were also considered. However, advances in computational and imaging technology have resulted in a paradigm change in photogrammetry over the years. This has completely changed the way of photogrammetric procedures, moving from traditional plane table photogrammetry (1851-1900) to analogue photogrammetry (1901-1950s), then analytical photogrammetry (1930-1980s), and finally optical (softcopy) photogrammetry (1990s-Present). In short, Photogrammetry has been used for about 150 years. Photogrammetry has progressed from a strictly analog, optical-mechanical technique to computational approaches based on computer-assisted mathematical algorithm solutions, and finally to digital or softcopy photogrammetry based on digital imagery and computer vision. Photogrammetry is mostly concerned with obtaining accurate measurements of three-dimensional structures and surface characteristics from two-dimensional images. The application contains coordinates measurement, distances measurement, heights, coverage, size, planning of topographic maps, and produce of DEM and orthophoto.

2.1.1 Photogrammetric Procedures

There are three different ways to derive photogrammetric output (Awange & Kiema, 2019): acquisition (analogue camera, photograph, scanner, digital sensor, and digital imagery), photogrammetric restitution (inner orientation, relative orientation,

absolute orientation, aerial triangulation, and map compilation or orthoimages generation) and photogrammetric outputs (photogrammetric product, 3D coordinates, orthoimages, DEMs, surface, and maps).

2.1.2 Data Acquisition

Analogue Frame Camera: the most common type of analogue camera used in aerial photogrammetry is the frame camera. Essentially, this is a metric sensor that operates from freezes/captures of a square region on the ground. It uses a typical format scale of 23 cm $\times$23 cm in most cases. The file base system is used by analogue frame cameras. The exposed film requires to be proposed the photograph. The high image accuracy of analog frame cameras is based on high geometric fidelity lenses with minimal lens distortion and application of film mounting tools to hold flat against the camera's focus field at the time of exposure. Camera accessories are also incorporated to ensure the overall functionality of the analog sensor works well.

Digital Aerial Cameras: successful mapping past applications dating back to the 1920s using analogue frame cameras. Digital aerial cameras have experienced short time operation around the year 2000.

Photogrammetric Project Planning: before implementing aerial photography, the first method is applied to consider is designing for a photogrammetric project. Providing the area to be mapped so that the user can evaluate it and the photogrammetrist can determine the various project parameters, such as overlap and side overlap requirements, photographic scale, final map scale, and instruments to be used, in consultation with the client. Typically, a photogrammetric project focuses on 3 steps: developing a flight plan (which must be followed when taking aerial photographs), preparing a ground control, field surveys (to ensure a high accuracy), and estimating costs.

2.1.3 Photogrammetric Restitution

Photogrammetric Restitution: Photogrammetry's main goal is to obtain useful geometric and other forms of knowledge from observing and interpreting photographic imagery. To derive 3D geoinformation from the iconic 2D imagery, the aerial photos that have been collected must be further evaluated and interpreted. Classically, this has been achieved by the process of photogrammetric restitution. Conceptually, this includes simulating and inverting the main photographic process, which can be done

with a plane table, analogue, analytical, or digital photogrammetric technique. The basic classical photogrammetric workflow can be define such as interior orientation (to reconstruct the geometry or bundle rays which were derived from images measured through camera calibration and included the principal point's coordinates (x_o, y_o), the calibrated focal length (c), radial lens and tangential lens distortion elements, film deformation, atmospheric refraction and earth curvature), relative orientation (to constrain corresponding conjugate rays in order to clarify that they intersect uniquely in space in order to form a stereo model), absolute orientation (to overcome the stereo model both scale and height datum using ground control measured by GNSS in order to correct absolute orientation and generate orthoimages), and aerial triangulation (to identify the complete exterior orientation parameters of each image in the photogrammetric block which includes the (X_o, Y_o, Z_o) coordinates of the location from the camera over ground, also the camera attitude which determine through the rotations ω, φ, κ, and to estimate ground coordinates (X, Y, Z) of measured conjugate image points).

2.1.4 Photogrammetric Output

Photogrammetric output is divided into three categories: photographic products (which are basically variants of single images or composites obtained from stereopairs), computational results (the DEM/DTM (DEM/DTM) is the most common method for representing height variations on the earth's surface), and maps.

2.1.5 Unmanned Aerial Vehicle

Unmanned aerial vehicles (UAV) commonly known as drones have become a "hot" topic, due to its advances and applications in remote sensing and photogrammetry applications. It includes technology, security concerns, rules, and regulations globally (Singhal, Bansod, & Mathew, 2018). Its application can have a military or a civilian purpose. Various missions can be done with UAVs e.g., estimations of land size, surveying or corridors for roads and railroads, stockpile volume estimates, flooding, and coastal erosion assessment, construction information management, emergency preparation and handling, surveys in remote or undeveloped areas, and goods delivery (Traore, 2021).

2.1.6 UAV Timelines

Unmanned aerial vehicle (UAV) are unmanned and is controlled remotely by a pilot on the ground. This enables to build small UAVs. It overcomes the terrestrial system's usability, speed, and reliability limitations. In defense, unmanned aerial vehicles have been used for reconnaissance and war(Singhal et al., 2018). The project on discovery of autonomous mechanisms started with Pythagoras, and it's attributed to Archytas of Tarantas. Based on geometrical concepts, they build the first UAV in 425 BC, and the mechanical bird possible to fly due to a mechanism placed in the stomach. In 1483, Leonardo Da Vinci had successfully designed an aircraft that was able to fly vertically. It is known as today's helicopter ancestor. Later Mikhail Lomonosov had designed an axial impeller in 1754 and Bienvenue Launoy created a counter model propeller in 1783. In 1840, Horatio Philips has designed a machine capable to fly in vertically routes, in 1849 the first use of unmanned combat air vehicle was designed by Baloane Austriece. Pontond Amecourt had built and flown smaller helicopters models, which powered from steam in 1860. In 1900, Nikola Tesla has presented the idea to control ballon wireless. During World War I, in 1916 aerial target was controlled from the ground flying with bomb has designed by Archibald Montgomery. In 1917 the aerial torpedo flew in automatic mode for US military representation designed by Kettering Bug. In 1924 was the first successful flight of RAE in 1921 designed by De Havilland. Reginald Denny led a project to develop a series of RPV in 1935 and later introduced a low-cost RC aircraft for training AA gunners in 1939. In 1944 Germans used a Fi-103 V1 known as cruise missiles during World War II. In 1941 the first aircraft flying unmanned from the scientific research Northrop and the first Jet engines were used. It was designed by Teledyne Ryan Firebee. In 1955, the first unmanned aircraft in reconnaissance had used by the US military and British company Beechcraft. In 1960 the first flight of an unmanned helicopter Gyrodine QH-50A was used in Maryland. In 1964, in the Gulf of Tonkin the U.S. has used a UAV in the conflict between the U.S. Navy and the North Vietnamese Navy. In 1966, D-21 was designed for use in reconnaissance missions over China and the recognition aircraft utility was demonstrated in Vietnam (Prisacariu, 2017). Singhal et al. (2018) has been documented of evolution UAV that in 1916, the Royal Navy used drones for gunnery practice, perhaps the first semiautomatic aero plane ever produced (aerial torpedo).

After that, with the introduction and incorporation of advanced navigation sensors, unmanned aerial vehicles (UAVs) became an essential part of the armed forces in 1933. The emergence of technology has not only eliminated the limitations of UAV exercises in the military, but it has also enabled them to extend their capacity in commercial applications such as agriculture, research activities, recreation, servile, transporting products, photogrammetry, and other purposes.

2.1.7 Classification of UAV

There are two types of UAV, which have been classified such as based on aerodynamics and landing, and weight and range (Singhal et al., 2018):

2.1.7.1 Based on Aerodynamics

Fixed-wing aircraft, chopper, multi-copter, motor parachute and glider, UAV with vertical takeoff and landing, congregating ready-made components, and commercialized UAV are some of the different types of UAV systems that have been built and are in the advancement process. Each one is assigned to a particular task and has its own set of zeros and ones.

Fixed-wing drones*:* are the most common one. They are saturated in design and production, which has led to the successful generalization of larger fixed-wing planes with minor modifications and improvements. Fixed wings are appropriate in response to higher air velocity and a steeper angle of air. When comparing fixed-wing and multirotor drones for the same payload, fixed-wing drones are more convenient, requiring less power, and having a thrust loading of less than 1. To control the orientation of an aircraft, rudders, ailerons, and elevators are used to control yaw, roll, and pitch angles. Fixed-wing drones are not possible to fly at a place and it is not possible to maintain their low speed. With a larger L/D ratio and a higher Reynolds number, fixed-wing drones are more efficient. On the other hand, they are less visible for L/D 10 because the Reynolds number and performance of smaller drones decreases.

Flapping wing drones: was inspired by insects such as small hummingbirds to large dragonflies. The lightweight and versatility of the wings were influenced by insect and bird feathers, which demonstrate the usefulness of weight and flexibility in aerodynamics. On the other hand, flapping wings are complicated due to their complicated aerodynamics. In a windy environment, flapping drones can support stable

flights in contrast to fixed-wing drones. The flapper motion is provided by light, flexible, and flapper wings with an actuation mechanism.

Fixed/flapping-wing: the result of combining the fixed and flapping mechanisms is used in situations where fixed wings are used to generate lift while flapping wings are used to generate propulsion. These types of drones are inspired by dragonfly which uses two pairs of wings for increasing the lift and also thrust forces. The main rotor blade of a multirotor produces a powerful thrust that is used for both lifting and propelling. Vertical takeoff and landing (VTOL) are possible with multirotor unmanned aerial vehicles, and they can fly anywhere. The number and placement of motors and propellers on the frame determine the multirotor configuration. Its moving ability to maintain a constant speed makes it suitable for surveillance purposes and monitoring. Multirotors require more energy, which limits their endurance.

Multicopter: has been divided into different categories based on the number and placement of motors. Each category belongs to a specific mission class, and the mission requirements. Monocopter, Tricopter, Quadcopter, Hexacopter (X, + configuration) Mode, Octacopter (X, + configuration) Mode, Octacopter (X, + configuration) Mode, Octacopter (X, + configuration) Mode, Octacopter (X, + configuration) Mode, Octacopter (X, + configuration) Mode, Octacopter (X, + configuration) Mode, Octacopter.

2.1.7.2 Based on Landing

Horizontal takeoff and landing (HTOL) and vertical takeoff and landing (VTOL): HTOL is a fixed-wing aircraft extension with a high maximum speed and a smooth landing. VTOL drones are experts at flying, landing, and hovering vertically. However, their maximum speed is reduced due to the slowing of retreating propellers.

2.1.7.3 Based on Weight and Range

Some researcher and organization have classified the drone based on their weight and range such as Nano (fixed wing and multirotor, 200g, 5km), Micro (fixed-wing and multirotor, 2kg, 25km), Mini (fixed-wing and multirotor, 20kg, 40km), Light (fixed-wing and multirotor, 50kg, 70km), Small (fixed wing, 150kg, 150km), Tactical (fixed wing, 600kg, 150km), MALE (fixed-wing, 100kg, 200km), HALE (fixed-wing, 1000kg, 250km), Heavy (fixed-wing, 200kg, 1000km), and Super Heavy (fixed-wing, 2500kg, 1500km). Commercial drones are now in global market such as Autel Premium

(1.6kg), Blade BLH7480A (95gm), Dji Product (1.2kg to 3.80kg), KAIDENG K70C (0.57g), Parrot ANAFI (0.32kg), PARROT BEBOP 2 POWER (0.525kg), JXD 509G(10kg), Quanum Nova (15kg), SYMA X8HG (~1.5 kg), Yuneec Tornado H920 (4.9kg), TYPHOON K (1.7kg), TYPHOON H+ (1.645), WALKERA SCOUT X4 (2.27kg), VOYAGER 3 (3.650kg), and KAIDENG K70C (0.579kg).

2.1.7.4 Designing Hardware of Unmanned Aerial System

The design of an unmanned aerial system includes the unmanned aerial vehicle and other subsystems a communication connection between the UAV and the operator, a ground control station, and accessories like a gimbal and a payload. The selection of components like the airframe, controller, engine, propellers, and power supply is critical and necessarily requires strong capabilities and full-fledged mathematical calculations to design a UAV for a particular task.

Aircraft design: the type of application determines the aircraft's design challenges, which include coverage area, maximum altitude, speed, climb rate, flight time or endurance, and stability. Even though maximum altitude is restricted by aviation regulations, higher altitude allows for a larger coverage area and increases survivability. Inertial measurement units, engines, propellers, and receivers, processors, and airframes are the main components of aircraft subsystems. Alloys, aluminum, and titanium are the most popular metallic materials used in aircraft construction, while non-metallic materials include transparent and reinforced plastic.

Ground Control System: made up of a wireless router and a computer that is used to collect, process, and data. Open system architecture, compatibility with various platforms such as airborne, ship, and land, real-time data execution, ability to monitor multiple UAVs, payload control, and contact with other ground control stations are all criteria for a ground control station. Other safety and security functions that can be anticipated from the ground control station include alerts and emergency response plans in the event of a malfunction, as well as power outage restoration.

Data Link: is the setup of a communication channel between the Aircraft sensors and ground control station (GCS). A wireless link IEEE 802.11 was used to connect between the aircraft's central data unit and the ground control station. Currently, antennas operate at 2.4GHz with a minimum gain of 12dBi. For online video

and picture transmission to a ground station, an additional wireless connection based on orthogonal frequency division multiplexing (OFDM) is used(Singhal et al., 2018).

2.1.7.5 UAV Data Collection and Analysis

Data collection, pre-processing of images, classification of images for feature extraction, measurement of mathematical equations based on the reflectance of images driven from drones such as Indices, and then the development of a suitable model for results visualization and analysis are all parts of the UAV data collection and processing process.

Data collection: flight planning, marking Ground control points (GCPs) for samples collected, and UAV flight are all automated. Correct pre-processing, which is required for the accuracy of UAV data, is a critical step in the creation of models. Image collection, accurate georeferencing, ortho-rectification, and mosaicking are all parts of the pre-processing of UAV data (aligning images using Image control points, point cloud, and GCPs). The supervised and unsupervised methods for planimetric feature extraction such as road, railway track, agriculture ground, forest, land cover, and water bodies are used in the classification of georeferenced UAV photos. The methods of maximum likelihood classification (MLC), random forest, and support vector machine (SVM) have been used. In the case of unsatisfactory results, manual classification can be tried. The results of the UAV have been implemented based on the case study; in general, this method of processing has been used for land use land cover classification, agriculture biophysical parameter determination, and soil study. The Normalized Difference Vegetation Index (NDVI), Green-Red Vegetation Index (GRVI), Soil Adjusted Vegetation Index (SAVI), and Modified Chlorophyll Index are some of the most widely used indices (MCI). Finally, users could generate models for a particular use in the case study(Singhal et al., 2018).

2.1.7.6 UAV Software for Images Processing

UAV software can be used to design flight plans, image processing, and data analysis for service providers and farmers to provide essential inputs for optimization and better decisions at a low cost. UAV software can be used for a variety of purposes, including mining, building, surveillance, rescue operations, and recreation. At the very least, good UAV software should include automation of UAV flight plans, augmented

view, geo-rectification of images, and the generation of 2D/3D models (Singhal et al., 2018).

A comparison of common UAV software on the global market are:

Aero Points: provides proper ground control points (GCP) for UAV surveys. It supports automated data upload, which is quick and simple to set up. However, it has some limitations in terms of features such as NDVI maps and the design of 3D models.

Agisoft Metashape: allows for the creation of 3D models and also photogrammetric processing. NIR, RGB, thermal, and multi-spectral image sensors are all supported by this cost-effective all-in-one software suite. In comparison to Pix4d, it is slow and limited in features. There is only one license for one computer.

Drone Deploy: can produce high-resolution charts, studies, and 3D models, and also real-time 2D Live Maps for fast analysis. It is better for agricultural applications and works with third-party UAV hardware and accessories. The surface detail for buildings limitation of this product is somewhat disappointing as compared to the more specialized solutions from Agisoft and Pix4D.

Drone Logbook: It can import flight logs and automatically fill in the information, and display GPS trace and replay it in 3D. Compliance and custom reporting, task preparation, and an operations schedule are all advantages of this program. This program, however, is unable to create digital elevation and terrain models.

Drone Mapper Rapid: Orthomosaicking, DEM, and a robust processing algorithm are all possible with free to download and test on a limited data set, but only capable of processing 150 images per scene.

Drone Mapper Rapid Expert: Up to 1000 geo-tagged JPEG images of 12 Mpixel format or greater can be input, with maximum photogrammetric functionality. It can generate X8, X4, or X2 DEMs and can use up to 1000 georectified images. The product's drawback is that it lacks self-calibration capabilities.

Field Agent: Sentera's AgVault is being replaced by an IOS Mobile device-powered automated flight with unlimited NDVI images, which enables users to scout crops in near real-time, capturing health and vegetation index data. The trial version of the mobile app is free. The complete version costs $29 a month.

Live NDVI: capable to use video technology for livestream NDVI video at the field's edge with real-time during flying drone. The limitation is compatible only with sentera double 4K sensor.

Pospac UAV: able for georeferencing directly and the post-processing software limited with maximum accuracy and efficiency. It is compatible with APX-15 L-UAV.

Pix4D: users can generate orthomosaics, point clouds, and professional 3D models with photo camera self-calibration and automatic DTM generation. Topographic maps can be done manually.

Photo Mod: provides all photogrammetric products like DEM, dDSM, 2D and 3D-vectors, and orthomosaics. This product is high performance with a simplified user-friendly interface and possible to automation of photogrammetric operations. Its limitation does not have the camera self- calibration facility, unlike pix4D.

Sensefly eMotion: designing flight planning and data processing is feasible. It can also connect wirelessly to drones, perform finger swipe flight planning in a complete 3D environment, and support multi-flight missions. While this product has advanced features, it does not have real-time NDVI processing.

Sense fly Survey360: the product is a complete aerial mapping system with accurate geo data that generates accurate point cloud and surface model outputs in a shorter amount of time. However, it does not provide a full three-dimensional model.

Ugcs: It can be used to create three-dimensional mission planning environments, prepare and fly projects without an internet connection, and it can support the majority of drones. It can also create routes from KML files and create in no-fly zones for major airports. However, it lacks real-time NDVI video, requiring the use of a graphics card with DirectX 9 support.

Virtual Surveyor: 3D visualization photogrammetry, virtual surveying, flight planning, and civil architecture are some of the services provided by the software. This product could be used for flood simulation, quick simulation, and interoperability with computer aided design environments. It can also handle large amounts of data files. Its drawback is that the virtual surveyor is not responsible for the information's reliability, precision, or suitability.

2.2 Basic of Height Measurement

Tree height is one of most important parameters used to estimate individual tree biomass and for forest monitoring and management purposes. To derive tree height there are two main techniques measuring tree height from field based or using remote sensing technology. The length of tree stem is an important part of any calculation of the total amount of wood contained within it. Furthermore, the height of the tallest trees is another essential factor in forestry. The vertical distance from ground level to the highest green point on a tree is described as its height. It may be difficult to define tree height in terms of stem length or to identify the height to the increasing point at the top of the stern. In addition, near the top of the crown of many tree species that it is hard to identify exactly what constitutes the stem, because of the dense growth of small branches near the tip. It's also difficult to determine where the top of the tree is. So, from the ground, while looking at a tall tree with a thick canopy. Although a tree's highest green point (tip) is much easier to recognize than its stem reach. In some cases, standing far away allows one to see the top clearly(West, 2009).

2.3 Tree Height Estimation

2.3.1 Field-Based Tree Height Measurement

There are three methods used to measure tree height such as direct, trigonometric, and geometric methods (West, 2009): The first method is direct height measurement: a pole and a telescope is used. The pole is direct1y positioned alongside the tree stem. The telescope is built in to record the height to which the pole has been raised. These are able to measure tree heights to about 8 m. The second method is height estimation by trigonometric method. The calculation is based on trigonometric methods. Certain variables need to be known before the vertical height of a tree standing on flat ground, the distance of an observer to a tree and the angel of the observer to the tree based height from eyes of observer to the tree. The third method is tree height estimation by geometric method. This method is similar to the trigonometric one. In contrast of using a telescope and poles, the observer needs a straight stick to know the length max. 3 m - 5 m. The observer uses a rule with standing convince far from the tree and not closing his eyes during using the ruler base on the stick to see the top of the tree.

Direct measurement of tree heights or field-based height measurements are possible with telescopic poles, tape, hypsometer, laser device, or total station. The accuracy and precision are limited to a tree height of 23 m. Moreover, this method is time consuming and uncomfortable. In addition, direct measurements are done by using destructive methods, which require harvested trees and are limited to the length of the measuring tape.

Non-destructive geometric or trigonometric methods have also been used which result possible to retrieve from measure tools such as hypsometer, laser device, or total station (Krause et al., 2019b). In the classical, individual tree height measurement method can be measured by climbing trees (Jurjević et al., 2020) or using telescopic poles(Van Laar & Akça, 2007). The telescopic poles are consisting of aluminum or fiberglass. They are used to measure the tree height up to 15 m. Hypsometers is a standard practice of tree height measurement. Their design is based on their construction theory. Blume–Leiss, Suunto, and Haga, and the Abney level hypsometers are trigonometrically related. Christen, Merritt, Chapman, and Vorkampff–Laue hypsometer have a geometric basis (Van Laar & Akça, 2007). Clinometers, hypsometers, orange finders have been documented as an indirect field measurement. Hypsometer or range finders are commonly applied in forest inventory (Bragg, 2014; Dobbertin, Neumann, & Schroeck, 2013; Skovsgaard, 2004; Van Laar & Akça, 2007; Wong & Tsuyuki, 2017). Classical direct methods have limitations in terms of high trees and scale accessibility. Indirect methods are more efficient for big areas and quantification of tree. Moreover, the enable the measurement of high trees. In order to obtain accurate tree height estimates with small errors, only qualified collectors should perform the work. They need good knowledge about the forest structure, tree species and height, surrounding topography, measuring distance and applied instrument. Experiences from the field showed still a high amount of random errors, hence, common instruments are based on the tangent method to reduce systematic error (Larjavaara & Muller-Landau, 2013).

2.3.2 Remote Sensing Tree Height Measurement

Remote Sensing (RS) are advance tools to use in order to seek for issue, producing information location, and analysis. Remote Sensing sensor collect data from the various location as capturing images using electromagnetic spectrum. It's also used

to investigate natural resource information which possible to see in visible or near-infrared (Andreo, 2013).

The development of Remote Sensing technology has also played important role in tree height measurement. Measuring tree height using indirect tree measurement or Remote Sensing is able to retrieve tree height. Traditionally, remote sensing technique uses photogrammetric measurements which we are possible to generate tree height from analog aerial imagery, digital aerial photogrammetry (DAP), active sensor remote sensing techniques such as Light Detection and Ranging (LiDAR), or Interferometric Synthetic Aperture Radar (InSAR) (Krause et al., 2019b). LiDAR technology was the principal experiment as remote sensing tools for topography and bathymetry in the 1960s. In 1970s, LiDAR was applied for forest applications and it is also the first investigated in the 1970s. In early 1980s, the interest in the accurate estimation of height forest stand, volume, and biomass have been developed, it was shown that the stand height estimates produced by LiDAR technology achieved accurately comparable with field observation, or the standard of photogrammetric measurements. LiDAR has been successfully used in estimating timber volume and biomass. In 1993, most of forest studies using LiDAR were successful with profiling systems. LiDAR applied either full-waveform or discrete return approaches. Since the Global Positioning System (GPS) had not yet completely established at the time, it was difficult to locate the LiDAR mark on the ground. Some researchers have been exploring LiDAR scanners with precision GPS and Inertial Navigation Systems (INS), also known as internal measurement units since the mid-1990s (IMUs). The stand height and volume measurements were comparable to those obtained with profilers. The new scanning LiDAR systems' return density allows for the resolution of individual tree crowns, enabling for the measurement of individual tree heights. The stand height and volume which other forest height includes forest parameters such as biomass and vertical foliage distribution begin to study(St-Onge, Treitz, & Wulder, 2003). Currently, LiDAR data has been used as tree parameters for extraction from LiDAR, which has applied field measurement to validate results (Ganz et al., 2019; SILVA et al., 2018; Su et al., 2012). Even though there are many studies applied LiDAR technology for estimation tree height, LiDAR data required high budgets which it may provide limitation to forest management(Moe et al., 2020) and another remote sensing

technology, satellite images are suitable to use for large scale only due to spatial resolution, weather condition and times (He et al., 2019). Unlike Lidar, new development of low-cost UAV produce high precise for retrieving canopy height and its crown coverage has been applied to obtain tree height from different types such as Pinus Pinea plantation (Guerra et al., 2016), Pine tree (A. C. Birdal et al., 2017), Pinaceae and Taxodiaceae (Lim Ye et al., 2015) , and Olive tree (Díaz-Varela et al., 2015).

2.3.2.1 The Use of UAV to Estimate Tree Height

UAV product has been successfully applied in different purposes for urban forestry (A. Birdal, 2016) and forest monitoring(Berie & Burud, 2018; Paneque-Gálvez, McCall, Napoletano, Wich, & Koh, 2014). Urban forest inventories are including information of species, diameter, condition, maintenance needs, location, height, growing class, etc. This information requires an update in specified time intervals in order to bring to decision making. The Indirect measurement is useful for inventory analysis with the UAV platform. It is the measurement and archiving of aerial imagery for future temporal comparison. UAV products (true color aerial photography, Near-Infrared photography and included LiDAR data, DEM, and thematic imaging) complete spatiotemporal analysis. They allow to detect changes over time with small UAV which are affordable and provide aerial imageries. Multi-temporal data collected from UAV will provide effective comparisons to clearly identify the change of landscape and enables monitoring of certain areas. Inventory and spatial comparisons will provide useful information about urban forest structures that will lead to more effective management decisions (A. Birdal, 2016). Pix4D software was used to create a high-resolution DSM. Using a orthomosaic and a 2 m wingspan fixed-wing UAV capture photographs covering 158 ha in a single flight. In this study, a consumer-grade RGB camera was installed to measure tree height. Other researchers used a low-cost 2D laser scanner carried by a hexacopter to estimate corn plant height. It is a low-cost scanner to derive height of plant as well as generation of canopy height model (CHM) from Dji Phantom 2 vision. The UAV flew 50 m above ground level, feasible to derive the tree height (Zainuddin et al., 2016). The estimation of tree height (2015) using a low-cost camera mounted on DJi Phantom 3 professional generated tree heights from two types of trees Picea abies of Pinaceae and Metasequoia glyptostroboides (M.

glyptostroboides) of Taxodiaceae. DSM was generated from Pix4D software to extract tree structure for tree height estimation. They successfully derived heights from both. It shows significant differences upon the fallen tree leaves. A study of mango and avocado tree heights was performed with a Dji Phantom 4. It derived tree height (CHM) from the DSM and DTM which are comparable to terrestrial laser scanner and airborne laser (Wu et al., 2020). The recent use of Dji Phantom 4 Pro for 24 hectares of mixed forest stand on a mountain area was successfully done. The altitude of the UAV was 120 m above ground level. It generated DTM and CHM for tree height estimations and were comparable to field observations (He et al., 2019).

2.3.3 Methodology for Tree Heights Estimation

Previous studies showed the successful application of different UAVs to obtain tree height from the Dji Phantom series such as Phantom 2 vision+ (Zainuddin et al., 2016), Dji Phantom 3 Professional(Lim Ye et al., 2015), Dji Phantom 4 (Wu et al., 2020), and Dji Phantom 4 Pro (He et al., 2019). The tree height was generated from the CHM which were derived from DSM and DTM. Pix4D has been used to identify individual trees using different methods. The super wide camera lens of Dji S800 which known as profession flying platform has been applied to derive CHM (Panagiotidis et al., 2017).

Zainuddin et al. (2016) has used Pix4D to process UAV images and generated CHM applied structure from motion SfM algorithm, and compared CHM with ground data. After the image processing, SfM has been used to export 3D point clouds to generate a Digital Elevation Model (DEM). Terrascan was applied to filter and remove noise from data points. Filtering and classification processes have been applied to create five categories ground, low vegetation, medium vegetation, high vegetation, and noise. Classified point clouds are capable to generate DEM from the noise class by removal unwanted data of ground. Fast binning approach use to create raster from las point clouds in order to create the DEM and CHM. The Minus geo-processing tool was used to generate tree height from the difference between DSM and DTM dataset. The result verification was applied the tangent method ($tree\ height = d_{hz}\ ((tan\theta_a + (tan\theta_b)))$), where d_{hz} is horizontal distance, and a = depression angle and b = elevation angle. The method assumed the tree base is directly above the treetop.

Lim Ye et al. (2015) used automatic generation ortho-mosaic images and DSM from Pix4D. In order to retrieved tree attribute estimation, the research goes through seven steps derivation of images and DSM from analyzing of stereo images in Pix4D software, extraction of tree area from otho-mosaic, subtraction of DTM and DSM to nDSM, combination of nDSM and otho-mosaic through layer stacking, segmentation of the stacked images, identification of the tree position and height, and comparison of results with field data.

Wu et al. (2020) used Pix4D mapper to process UAV images. Point cloud was densified before the classification. They also use Pix4D to classify the ground points using a machine learning algorithm. The applied triangulation method was the Delaunay triangulation algorithm. The algorithm performs two steps removal of outlier and matches refinement. It can be used to generate DSM and DTM. The DTM and DSM is created by interpolation of classified ground points. In order to produce CHM, they differentiate the distance between ground and tree top by subtraction of DTM from DSM. The 3D point cloud was automatically georeferenced through geotags embedded in the photos, however, to improve the horizontal georeferencing accuracy which the CHM was then georeferenced based on the CHM from the Terrestrial Laser Scanning (TLS) data. Finally, a maximum CHM value for each tree crown was computed for comparison with the canopy height estimates from the TLS data.

He et al. (2019) conducted an observation in a complex terrain to extract forest structures in a mountainous area as well as tree height estimation. The study contained several steps. Firstly, the reconstruction of 3D point clouds and creation of a high-resolution DSM using photogrammetric technologies. Secondly, they used automatic classification of point clouds to generate DTM. BEP extraction and RBF neural network-based interpolations were used to produce high value pixel to represent DSM and by subtracted from DTM. Third, the individual tree height estimated from the CHM applied moving smooth window filter method-local maxima under a contour-surround constraint. Last, evaluation of the accuracy from the estimated and measured variables.

Panagiotidis et al. (2017) proposed tree height estimation by extracting DSM and DTM. DTM were derived by auto-classification from sparse point clouds. DSM were obtained by reconstruction of complete dense in Agisoft PhotoScan photogrammetry software. They applied the morphological filter-focal statistics tool in

ArcGIS to identify local maxima. The morphological filtering is required to identify the highest pixel value from the treetop of the CHM. Some pixels indicated multiple local maxima in a single crown area. The researcher applied adaptive filtering method based on CHM height values to identify individual tree positions.

A. Birdal (2016) has shown various methodologies for single-tree detections which test comparatively LiDAR data-based methods. They show the results of forest structure deeply affect the performance of all algorithms. Density and clustering were successfully applied in tree detection. The algorithms are differing which is mostly found in tree detection rather than height estimation. In the study, point clouds were retrieved from UAV aerial imagery and processed using LiDAR methods to obtain individual tree heights in a forest. Cluster formation using modified k-means approach which using ground-based training data. A Euclidian distance criterion was used to remove the unwanted local maximums. Local maximums were pretended as seed points. Based on these points, a k-means vector quantization algorithm is used to cluster the point data. Training data-based height reduction factor is used to lower the bias to improve the clustering of similar objects. A voxel layer single tree modeling algorithm: the algorithm works base on density images which are calculated from consecutive height layers that are extracted from point data projected into a voxel space. Images were traced with a hierarchical morphological algorithm from top to down assuming there occurs a tree crown when higher amounts of points are traced. Adaptive segmentation based on Poisson Forest stand model: this method is a pit-filling algorithm for Canopy Height Model (CHM) which applies a low-pass filter with a binominal kernel. It depends on the distance between the nearest neighbors. The distance needs to be estimated. Each ground training data CHMs, enables to interpolate various resolution to seek smallest tree crowns. Local maxima detection with residual height adjustment: the method uses the first return of point cloud data to interpolate and generate a DSM with different resolutions that are based on the training data. The DSM is smoothed from applying a 3x3 Gaussian filter by a number of times which assumes the DSM is pit-free. The first returned heights of the DSM are calculated using a percentile residual height distribution. The window size, the number of Gaussian runs, and the residual height percentile adjustment are set specifically for each study area which is based on the ground measured tree height and position. Segmentation based

on geometric tree crown models: computing the correlation between point cloud data and a geometric tree crown model which is placed at the center of a pixel known as the basis of this algorithm. A result of the images created with this correlation is possible to use in tree detection by marking each raster cell with a non-zero CHM value and a positive correlation value as seed points. Until a local maximum is found where a seed doesn't have a high correlation with neighbor seeds, these seed points are updated to the neighbor cell that has the highest correlation. The final seed is characterized as the tree crown segment. Adaptive filtering based on CHM height values: CHMs apply low-pass filtered using Gaussian kernels. CHMs are required to interpolate into a grid of desired values i.e., 0.5 m by using the maximum of the first return in the related grid. The empty cells in the CHM are filled by filtering the CHM with a defined window size by taking the average of pixels within the window. The algorithm has a pre-requirement of defining window sizes and height classes to produce results.

2.3.4 Method Comparison of CHM Retrieved from LiDAR and UAV

LiDAR (Light Detection and Ranging) is a remote sensing technology to generate detailed 3D structure information. The results from a 3D structure can be used for tree height estimation. Su et al. (2012) showed different methods of various researchers to estimate tree height using LiDAR data. CHM was used to estimate the height. CHM can be used to find differences between DSM and DTM. LiDAR provides good information about the height of non-ground objects like trees, road buildings, vehicles, etc. Various methods were used to smooth CHM in order to generate tree height estimation e.g., the Gaussian smoothing method. They used a recognition algorithm to detect the canopy cover, and a maximum search algorithm to recognize crown tops. Popescu, Wynne, and Nelson (2002) applied different moving windows of local maximum filtering to find the highest values which represent single trees estimate. The moving window commonly uses 3x3, 5x5, and 7x7 pixels. They suggested that choosing the correct filter window size is related to tree location estimation. If the filter size is too small or too large, it will affect the prediction. Most commonly used sizes are 3x3 and 5x5 (Daley, Burnett, Wulder, Niemann, & Goodenough, 1999; Wulder, Niemann, & Goodenough, 2000).

Unmanned Aerial Vehicle (UAV) is a passive remote sensing technology to derive tree height accurately. Obtained data can be compared to Airborne Laser

Scanning (ALS) (Krause et al., 2019b). CHM was applied to estimates tree height. It was retrieved from different photogrammetric software to generate ortho-mosaic, point cloud, DTM and DSM. S. Krause, T. Sanders, J.-P. Mund, and K. Greve (2019a) created CHM by interpolating the nearest neighbor of point cloud (DTM) merged with ground data. In this study, photogrammetric software was used which is based on DTM and DSM like Pix4d software (Hartley et al., 2020; Zainuddin et al., 2016). CHM identifies tree tops by calculating the difference between DSM and DTM. Local maximum was applied in various studies as well (He et al., 2019; Lim Ye et al., 2015; Wu et al., 2020; Zainuddin et al., 2016).
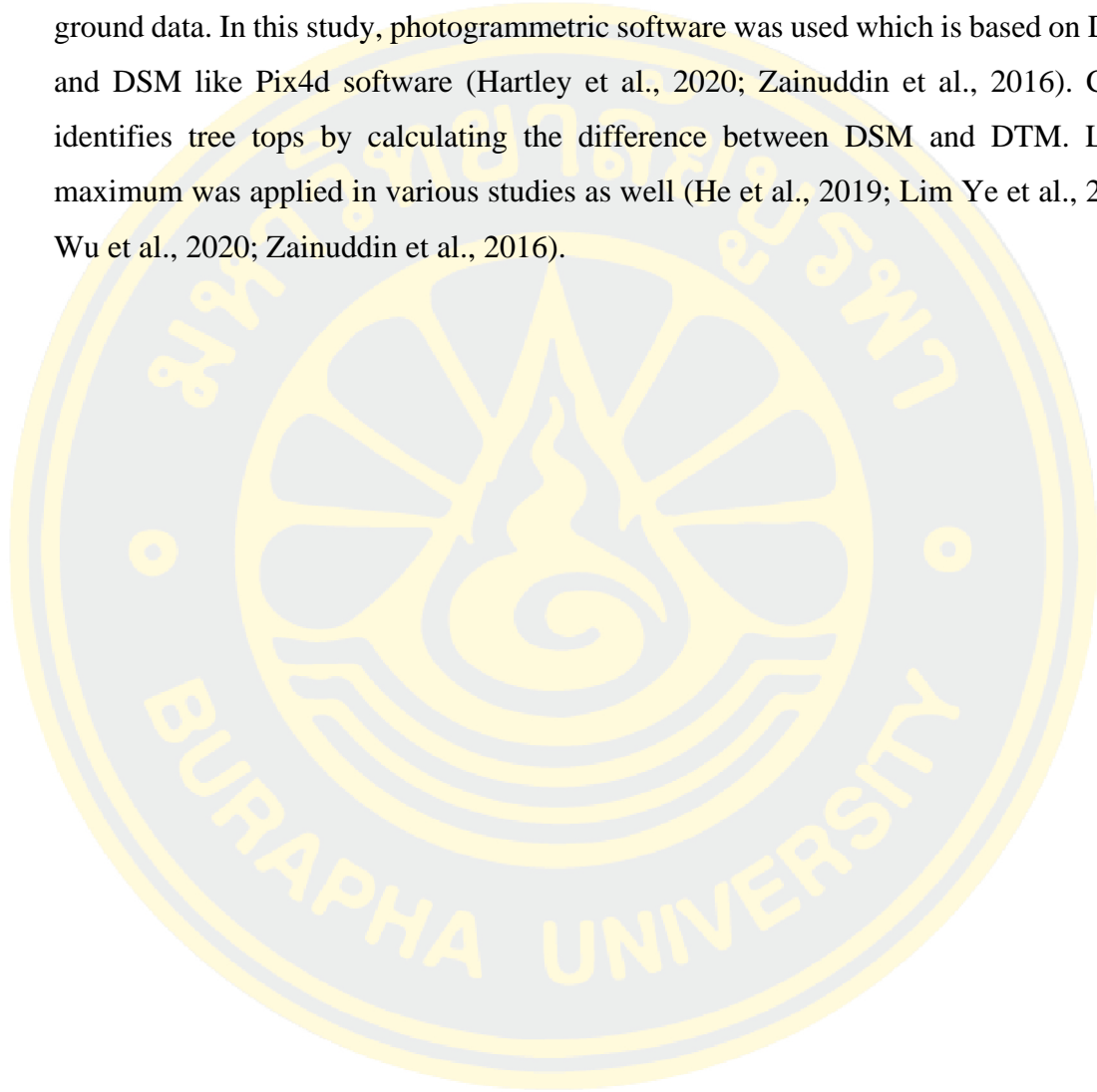
CHAPTER 3
RESEARCH METHODOLOGY

In this chapter, we are going to present our data processing, our results and draw the conclusion respectively to the flow chart in figure 1. First, our UAV images were processed in PiX4D which automatically generated DTM and DSM based on an approach SfM and Multi-View stereo (SfM-MVS). CFS filter were applied to differentiate ground and vegetation point clouds. The classified point clouds ground and none ground were converted to DTM and DSM. Canopy Height Model (CHM) were calculated by subtraction of DTM from DSM. Tree locations contained a buffer from field data collections. They were used as input features to extract the tree height from CHM. Furthermore, an evaluation of tree height was performed by comparison to field measurements in statistical analysis.
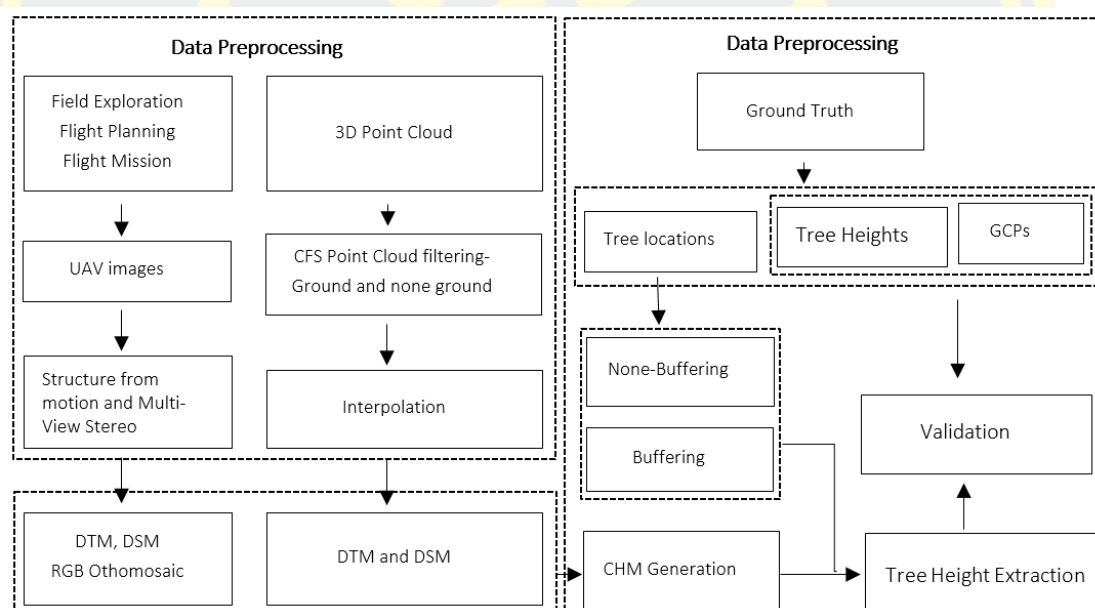
Figures 2 Workflow Diagram for Extracting Tree Height from UAV Data

3.1 UAV Platform

   A DJI Phantom 4 Real-Time Kinematic (DJI P4 RTK) was used in this study. The UAV capture images of 20-megapixel RGB true color images through a 1-inch Complementary Metal-Oxide-Semiconductor (CMOS) sensor consumer-grade camera with a field of view (FOV) of 8.8° and a focal length of 8.8 mm (35 mm format equivalent). The maximum flight time is 30 minutes with a maximum flight range of 7 km (He et al., 2019). In addition, this DJI product includes RTK which provides positional accuracy of less than 2 cm.

3.2 DGPs Platform

   Two types of DGPs were used emlid reach and E91. Low-cost RTK global navigation satellite system emlid reach signal tracked (GPS/QZSS L1, GLONASS G1, BeiDou B1, Galileo E1, SBAS) and 72 channels with LoRa ration. It can work up to 8 km from base station and up to 30 hours in standby (Emlid, 2019). In order to get precise data of ground positioning via reach view, 2 apps were connected emlid reach. This product has been used in earlier studies to assess the accuracy of Dji Phantom data (Meghani, Miller, & Holderman, 2017) and in the evaluation of low-cost GNSS Receivers (Jackson, Saborio, Ghazanfar, Gebre-Egziabher, & Davis, 2018). E91 GNSS receiver product has a dual frequency with 624 channels with strong signals (BeiDou B1, B2, B3; GPS L1, L2, L2C, L5; GLONASS L1, L2; GALILEO E1, E5A, E5B; QZSS L1, L2, L5; SBAS L1) and can be used in standby up to 16 hours which allowed to work with it using Landstar 7 apps (CHCNAV, 2018).

3.3 Photogrammetry Software

   In this research, Pix4D was used which was founded by a Swiss company in 2011 (®Ecublens, Switzerland) It is widely known as an image photogrammetry software. This software has become the main provider and applied for industry standard. The application of Pix4D is automatically divided into three steps: initial processing, point cloud densification, and DSM and orthomosaic generation (Ivosevic, Han, & Kwon, 2017). It used structure from motion and multi-view (SfMMVS) to generate output data like 3D point cloud with average density larger than 4000 points/m^3, DSM, and othomosaic. First, the software recognized and tie key points automatically about median. Roughly, 70000 key points per image. Second, buddle adjustment applied to do the camera parameters which calibrates each image

automatically. Then, the software generates a spare set of 3D key points. Last, multi-view approach used to create densified point cloud in high resolution and estimate point positions. To improve accuracy, images were referenced with GCPs. Among others, the output were a DTM applied inverse distance weighting (Navarro et al., 2020).

3.4 Study Area

Phnom Kulen National Park (PKNP) is located 48 km from Siem Reap Province and covers 37,380 ha. It is located in northwestern Cambodia. This location is a prominent archaeological observation site, a critical area for biodiversity, and a key component of the regional watershed (Singh et al., 2018). Land cover is primary regeneration and secondary forest. In the southern part, the cover mainly consists of cashew and cassava plantations (Singh et al., 2019). There are two main problems which have been documented related to forest management issues erosion linked to loss of forests and increase of agriculture. Hence. 8000 people have moved and lived on the mountain recently. Since 2005, farmland turns into crop land which are mostly cashew plantation (Cambodia, 2017).
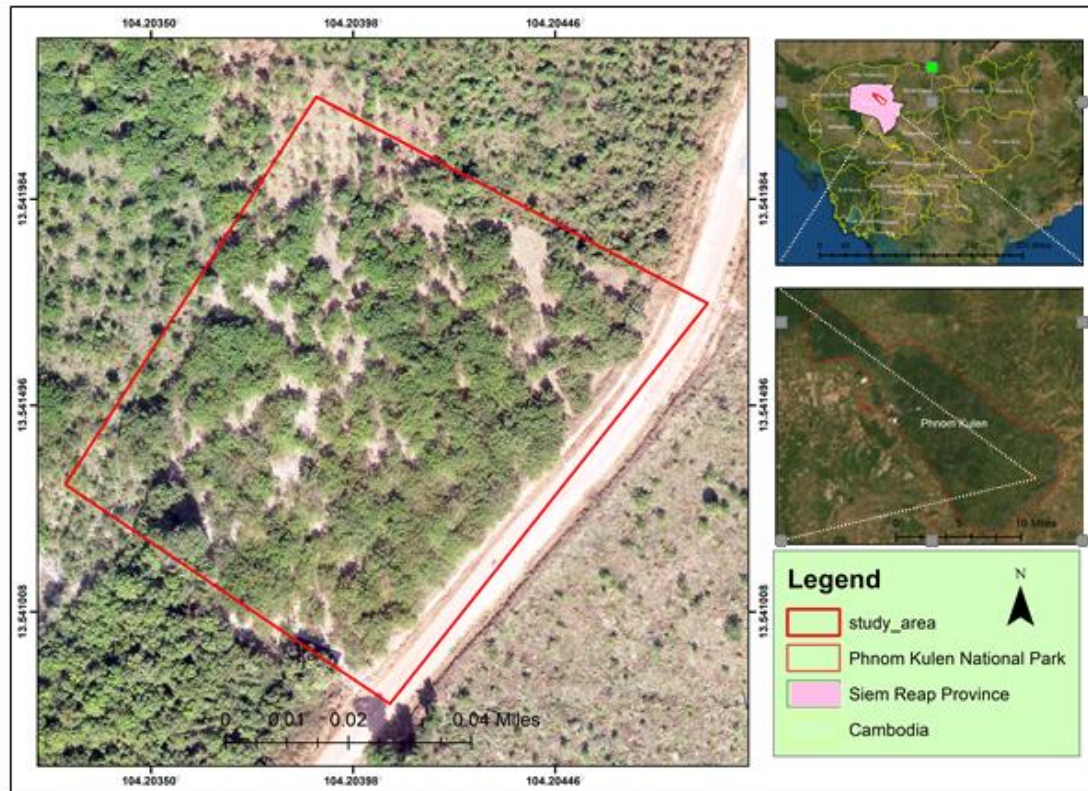
Figures 3 Study Area at Phnom Kulen National Park

3.5 Field Exploration

Google Earth Pro was used to identify the study area and to plan fieldwork. The selected area was an example area of the local region. It was suitable for necessary experiments, GCPs placement, and tree height measurement. Before the first flight missions, it was noticed that our UAV has a very strong effect of the antenna near our sites (Figure 4), hence, the UAV could not cover the planned study area. The mission was relocated to the center of the plot.

Figures 4 The Antenna That Block UAV in Flight Mission

3.6 Flight Planning and Flight Session

The UAV required good weather conditions to fly. The flight altitude was 50 m and 120 m above ground level (AGL) (He et al., 2019; Zainuddin et al., 2016) to compare estimated results of different flight attributes. It was proposed to fly at 50 m and 200 m AGL to cover approx. 1 ha. Planning of the Flight was first to create KML files based on google earth pro which were imported into the controller. Mission plans from KML in GS RTK could be used by the build-in app of the controller. The flight path automatically generates the start and end point in the study area. Flight attribute such as the altitude was typed in separately with a flight speed of max 3.9 m/s. Side overlap rate was 70 % (Zainuddin et al., 2016). Forward overlap rate was 80 %. Camera

ratio was 3:2. White balance was set to sunny and the camera angle was -90. There are 133 images and 39 images retrieved from the flights. The flight time was approx. 5min to 6 min (Figure 5).
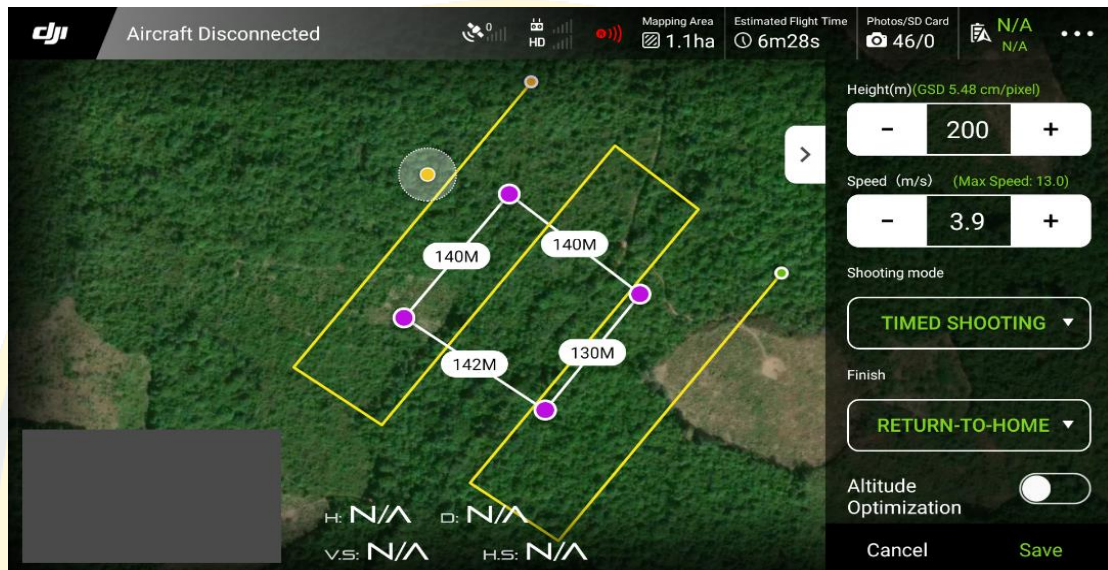
Figures 5 UAV Settings in GS RTK Application Applied in Research

3.7 Field Measurement

Ground truth data were collected at the same time with UAV images during 28 of March 2021. Two ground truth data sets were collected Real-Time Kinematic Global Positioning System (RTK GPS) receiver as reference data for selected 5 GCPs (4 at the corner and one in the middle) and 4 checked points respectively to Pix4D recommendation which more GCPs not mean more accuracy based on accuracy analysis (Pix4D). GCPs and check points were 150 cm x 150 cm. They were sprayed on the ground with red color. Tree heights were measured with 30 mm PVC pipes (Figure 6) which were removable. Tree height measurement by following the far angle to see the top of the tree respectively to trigonometric methods (M. Ramli & K. N. Tahar, 2020) with tree position also used RTK GPS (Emlid Reach and E91 product) to determine in 50 tree random points in ArcGIS software.
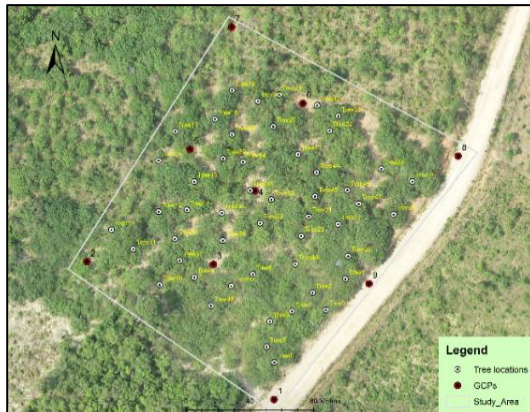
a) 50 tree locations selected b) GCPs designed

c) Tree height measurement d) Measuring top of tree

Figures 6 GCPs and Tree Locations from Field Measurement

3.8 Image Processing

The images from the 50 m flights above ground level and 200 m flights above ground level were processed differently. The UAV data were processed in three steps in Pix4D initial processing, point cloud densification, and DSM (Ivosevic et al., 2017). First, data input to Pix4D while the input was defined to WGS 84 and the output was defined to WGS 84 UTM Zone 48N, EMG 2008 geoid. Those were processed as 3D maps. After initial processing, GCPs were marked to georeferenced images. In the second step, a half image was applied to set the image scale to default. The optimum was set in point density with at least 3 matches. Point clouds were classified simultaneously. The processing was continued by two different methods (Figour 7). Key point extraction and camera calibration were done automatically using advanced

automatic aerial triangulation (ATT), Budle block adjustment (BBA), and a spare 3D point cloud which was computed. After 3D point cloud and textured mesh generation, an output-orthomosaic and DSM and DTM from point cloud classification were obtained.

Tables 1 Pix4D Functions Used in Each Processing Steps

Processing Functions	System Processing
Initial processing	Advanced automatic aerial triangulation (ATT), Bundle Block Adjustment (BBA), and spare 3D point cloud
Point cloud mesh	Dense 3D point cloud and a 3D textured mesh.
DSM, Orthomosaic	Generation the DSM, DTM, orthomosaic,
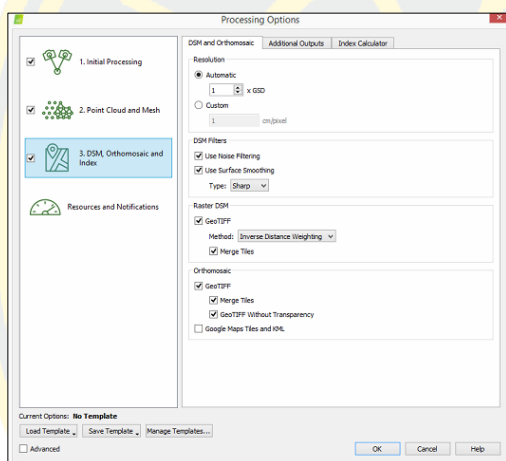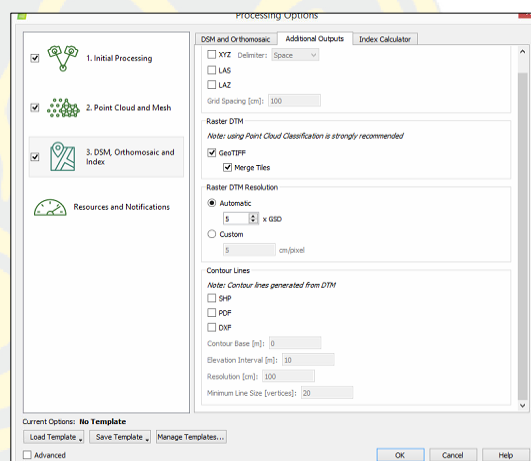
a) Default settings DSM generation   b) Default settings DTM generation
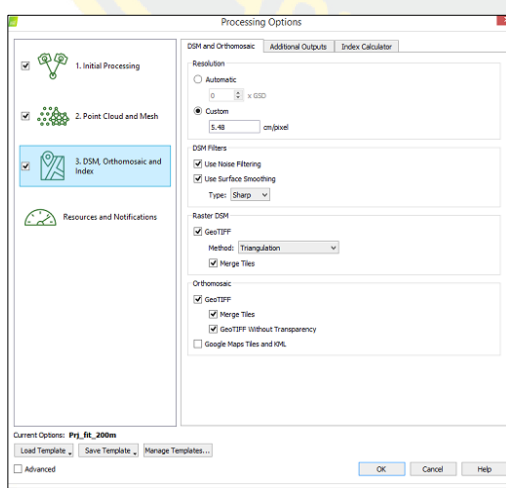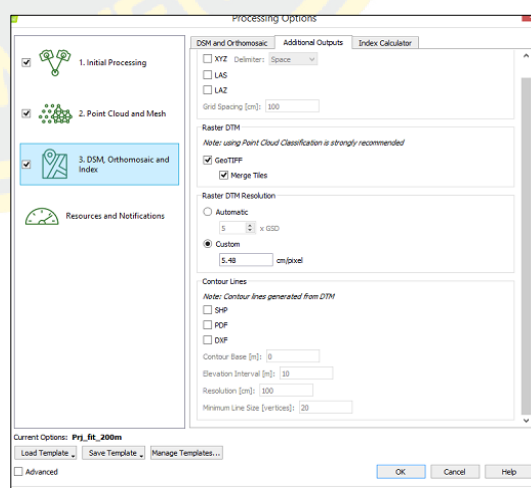
c) Default settings DSM generation   d) Default settings DTM generation

Figures 7 DTM and DSM Generation Settings Used in This Study

The used methods were:

- Processing was done with default settings method DSM generation using resolution 1 xGSD, Inverse distance weighting (IDW), applied noise filtering and sharp for surface smoothing, and DTM generation at default resolution 5 xGSD.

- Additional processing was performed with customized settings. DSM generation was changed to a resolution of 5.48 xGSD for both flights due to software limitations of GSD. While the original flight from 50 m had a resolution of 1.37 cm/pix, triangulation, applied noise filtering and sharp for surface smoothing and DTM generation at resolution 5.48 xGSD the same as DSM.

Each processing step was quite long consuming. The 50 m flights were processed with two methods as mentioned above which were the same as for the 200 m flights.

3.9 Point Cloud Classification

Extraction of semantic information can be done by two methods. The first method consisted of a segmentation of coherent objects from a scene. The Second method was assigned to class based on our images to each point (Becker, Rosinskaya, Häni, d'Angelo, & Strecha, 2018). Point cloud classification is mostly used with LIDAR data to generate 3D city models, 3D building models, building extractions, DTMs, and chang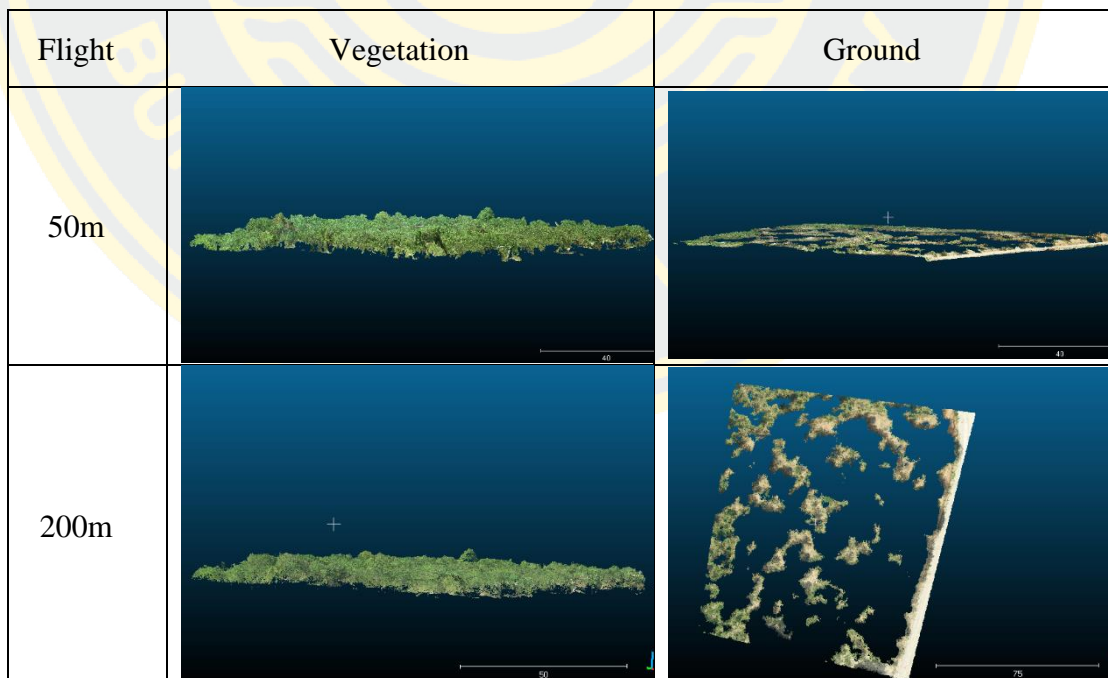e detections (Yastikli & Cetin, 2016). The LIDAR point cloud standard classification was introduced by the American Society for photogrammetry and remote sensing (ASPRS) (Table 2) (Graham, 2012). There are many software's used to process LiDAR data for visualizing and analyzing, but the accuracy differs and depends requirements (Fernandez-Diaz et al., 2008). One common software for tree height estimation by point cloud classification is lastools. It is available in https://rapidlasso.com/lastools/ (A. C. Birdal et al., 2017; Chan, Fung, & Wong, 2021; Jin, Oh, Shin, Njungwi, & Choi, 2020; Marcu, 2018; MILLIKAN et al., 2019; Ojoatre, 2016). Even though this software was successfully applied for point cloud classification and tree height estimation, there are limited functions for users. Free functions are laszip, lasindex, lasvalidate , lasinfo, las2las, lasview, lasdiff, lasmerge, las2txt & txt2las, and lasprecision while there are many more function with a license blast2dem,

blast2iso, lasground, lasheight, lasclassify, lasgrid & lascanopy, lasboundary, lascontrol, lasclip, lascolor, las2shp & shp2las, lasoverlap, lasoverage, lasduplicate, lassplit, las2tin, las2iso, las2dem, lasthin & lasnoise, lassort, and lastile(Engineering, 2015). Lastools functions for tree height estimation and point cloud classification requires to purchase it to differentiate between ground and none-ground (Tong et al., 2020). It was proposed to apply cloth simulation filtering (CFS), cloudcompare v2.12 alpha 64 bit which is open source software. Cloth simulation was introduced by Zhang et al. (2016). The algorithm is able to define ground points from LiDAR points clouds, while the input point cloud goes up and down, a cloth drop arranges low values points from high values points. Then it evaluates the arranged points based input data. The finalized results are ground and none-ground (Girardeau-Montaut, 2016). In addition, cloudcompare compares two points ground and none ground by using cloud to cloud or C2C (compare the nearest neighbor cloud to cloud), C2C_HF (nearest neighbor distance with height function model), and C2M (compare cloud to mesh) (Lague, Brodu, & Leroux, 2013).

Flight	Vegetation	Ground
50m		
200m		

Figures 8 Point Cloud Cleaning from 50m Flight and 200m Flight

Flight	CHM	Point cloud densities
50m		Vegetation : 6 627 708 Ground : 1 805 856
200m		Vegetation : 411 330 Ground : 103 874
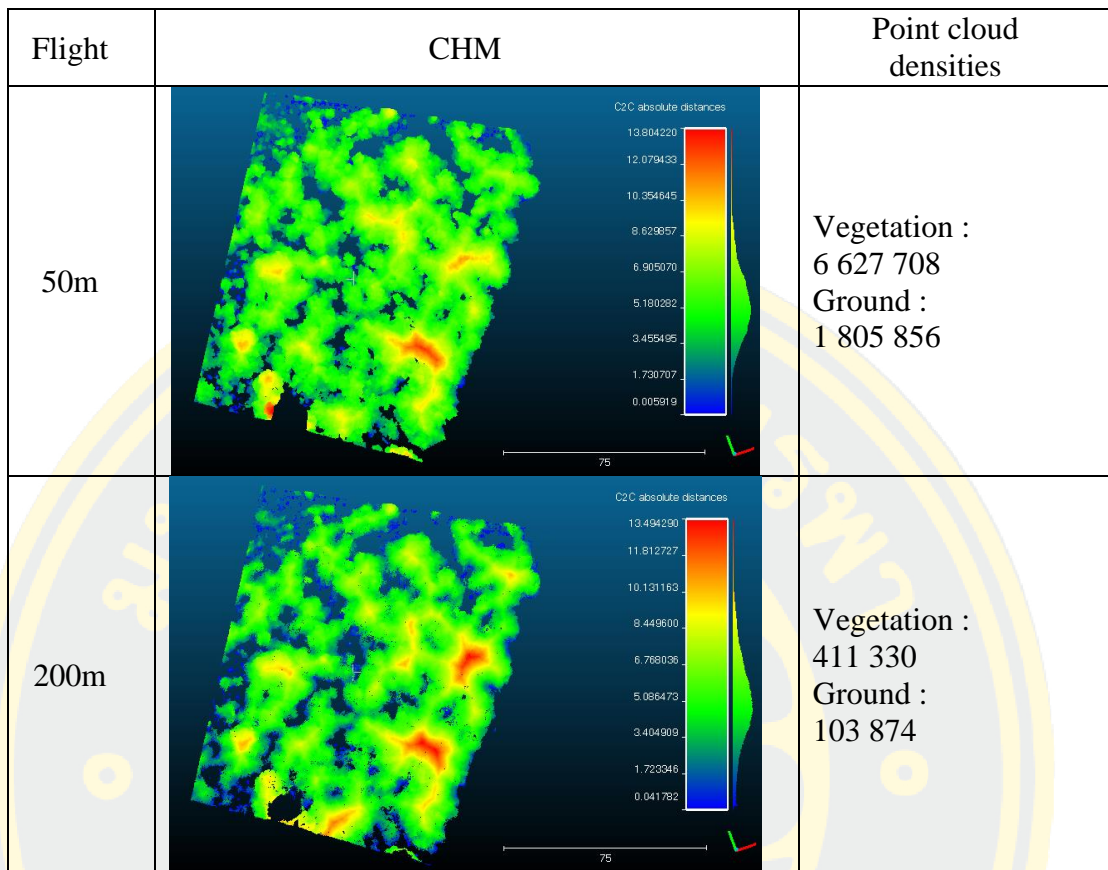
Figures 9 CHM Distribution from 50m Flight and 200m Flight in Cloud Compare

Tables 2 LiDAR Points Cloud Classification Standard Codes

N^0	Code Value	Meaning
1	0	never classified
2	1	Unassigned
3	2	Ground
4	3	Low Vegetation
5	4	Medium Vegetation
6	5	High Vegetation
7	6	Building
8	7	Low noise
9	8	high noise
10	9	Water
11	10	Rail
12	11	Road Surface
13	12	Bridge Deck
14	13	Guard
15	14	Conductor
16	15	Transmission Tower
17	16	structure connector
18-64	17-63	Reserved
65-256	64-255	User definable

3.10 DTM and DSM Generation from las File

The las classified, applied ArcGIS tool to convert it to a raster. First, las datasets were created by input las data. The result was lasd format which can be displayed and filter our point cloud data. In the next step, a raster was created by las dataset to raster. The file value was set to elevation. A binning approach was included and assigned to the nearest cell which is the void fill method as natural neighbor. The raster was resampled to 10 cm which is the same as the output from photogrammetry software. The interpolation mainly depends on the characteristics of the data. The comparison of two interpolation methods Kriging and inverse distance weighted (IDW) studied by Romero-Toro-Gascueña et al. (2011) showed that kriging provides less errors than IDW. Another experiment of Montealegre, Lamelas, and Riva (2015) found that triangulated Irregular Network (TIN) to raster interpolation and IDW were the best result for interpolation. Jurjević et al. (2020) generated 50 cm resolution of DTM using the binning approach. Guerra et al. (2016) applied natural neighbor interpolation method after point cloud classification same as Osińska-Skotak, Bakuła, Jełowicki, and Podkowa (2019) which applied natural neighbor to generate DTM and DSM as well. In this study, the initial results of the pre-processing, application of interpolation methods, showed that mainly the natural neighbor results are comparable with other interpolation methods in ArcGIS.
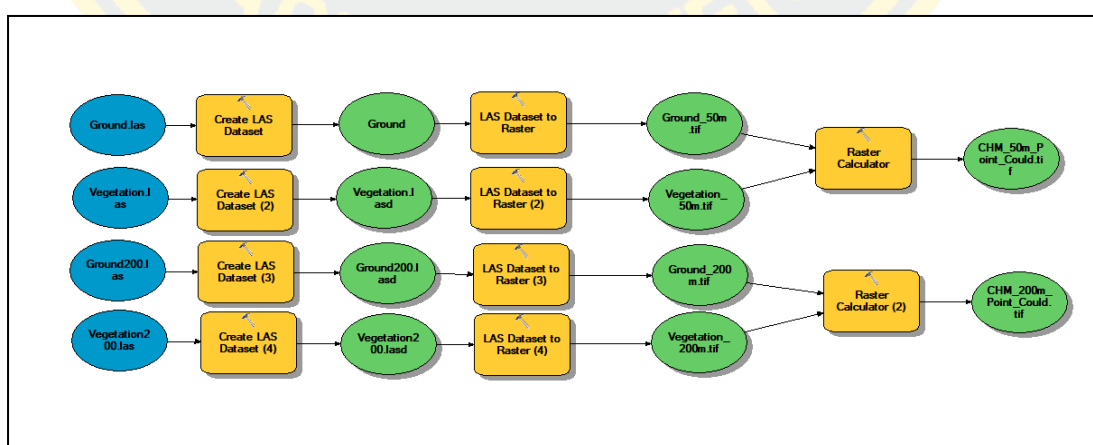
Figures 10 CHM Data Processing and Extraction From las Files

3.11 Buffering Tree Location

He et al. (2019); Panagiotidis et al. (2017); Zhou, Wang, Di, Lu, and Guo (2020) applied local maxima to generate seeds at the treetop, the highest pixel value treetop were derived by CHM. This method was challenged with cashew crown covers which have complex leaves. In addition Tian et al. (2019) proposed two new methods of crown cover area to extract tree height, individual tree localization (ITL) and canopy height model (CHM) seed points (CSP) were discussed. The ITL is based on DEM raster localization with a grid size of 20 cm $\times$ 20 cm and was used to automatically identify and mark center of grid after calculating tree height. Tree crown and center of tree are challenging which may affect the extraction results. In the present research, extraction of tree height were based on tree locations which were collected during field work. There were 5 buffer ranges applied 0 cm, 50 cm, 100 cm, 150 cm, and 200 cm (Figure 11). 200 cm was the maximum tree crown of 200 cm.
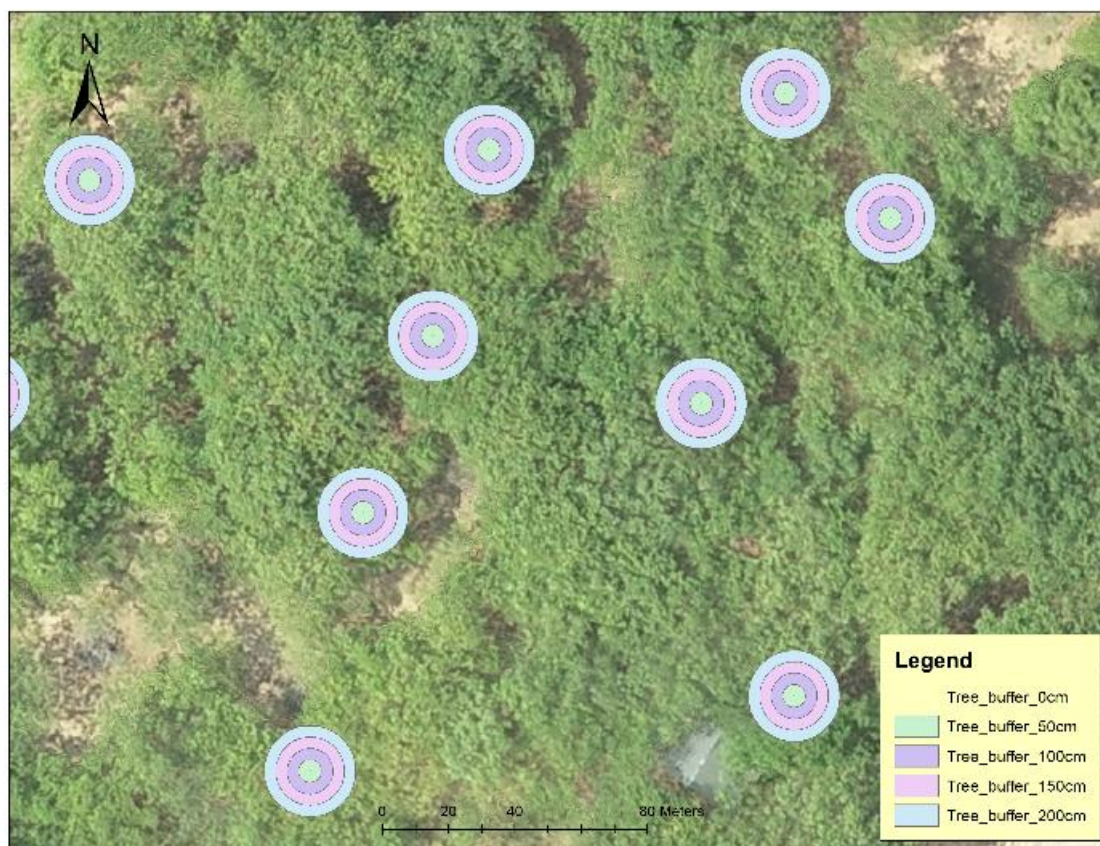
Figures 11 The Buffering Tree Locations Applied in Our Experiments

3.12 Canopy Height Model (CHM) Generation

3.12.1 Canopy Height Model Calculation

We first import the output of UAV images into ArcGIS desktop, and then generated CHMs by identifying the DSM value in each pixel by subtracting ground point represent DTM value which is possible to be calculated as follows (Equation 1):

$$CHM = DSM - DTM \qquad (1)$$

Where CHM is canopy height model, DTM is digital terrain model and DSM is digital surface model.

CHMs are generated using Equation (1) in order to find the height value of the DSM in each pixel and subtracting the corresponding DTM value(Zainuddin et al., 2016). When the DSM value less than the DTM value, so the CHMs value in a pixel is set to 0 (He et al., 2019).

3.12.2 Individual Tree Height Extraction

The tree height was defined from above ground height model and real height. It was interpreted by human eyes. In order to estimate individual tree height from ground, most previous studied applied filtering methods to the above ground height model which stored were in a raster format. This was done by applying a local maximum or the morphological filter-focal statistic tool in ArcGIS which focal statistics known as a filtering tool that possible to identify treetop location based on a maximum value (Panagiotidis et al., 2017). Examples of a previous study A. C. Birdal et al. (2017)Birdal, Avdan [15]Birdal, Avdan [15]Birdal, Avdan [27], they experimented to point out differences between the kernel and the circular-shape areas selected. Radius kernel was successfully applied at 8 kernels while testing kernel ranges of $rm \in \{1, 2, 3 \dots 18\}$. It was experimented various neighborhood operation from focal statistic calculation (majority, maximum, mean, median, minimum, minority, range, standard deviation, sum, and variety) in order to compute the best output raster in a specified neighborhood around a location. In addition, they have applied a conditional tool (Con), in order to match the pixel values (Equation 2) between CHM and focal statistic result. The conditional if/else was used to remove 0 value from pixel and assigned value to 1.

$$Con\ ('CHM'=='focal\ statics\ result',\ 1) \qquad (2)$$

Where Con is conditional tool, CHM is canopy height model and focal statics result is result from focal static tool in ArcGIS.

The selected tree cannot be applied to local maxima to identify treetops. The result was too many seeds generated from moving window and this method seemed not work well in the present research. Therefore, the buffer tools in ArcGIS to extract tree height were assigned to tree locations. Zonal statistic (Hentz, Dalla Corte, Netto, Strager, & Schoeninger, 2018; Zainuddin et al., 2016) was applied to extract tree height based on input features from buffers and input CHM which represent tree height. It was used for evaluation which considered to be the treetops compared with ground truth data.
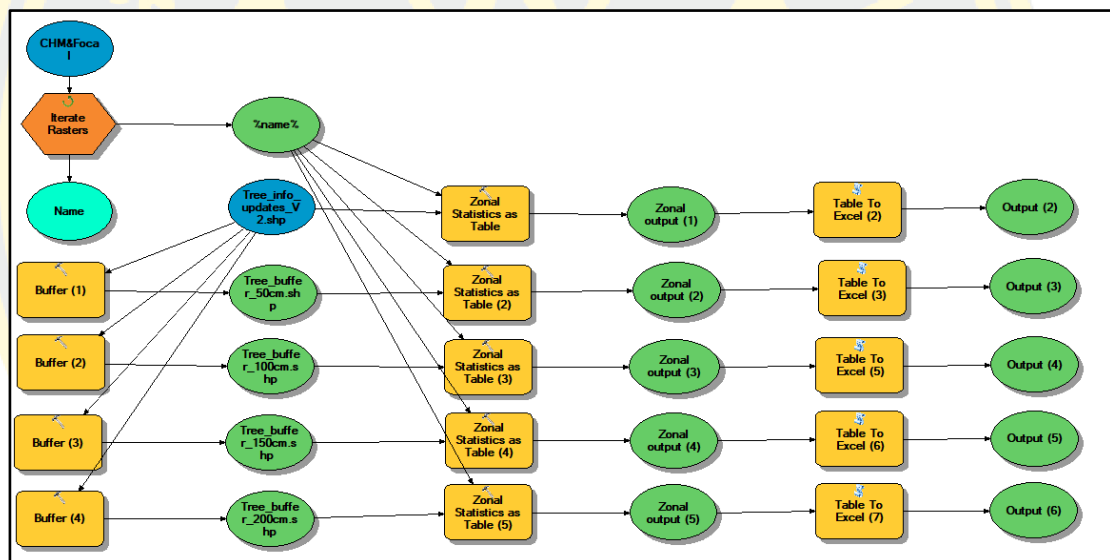
Figures 12 CHM Extraction Model for Both 50m Flight and 200m Flight

In this study, ID was used to represent our extractions from different experiments, tree heights from photogrammetry product and point cloud classification). Results from the 50 m flights were marked with an "A". "B" was assigned to the results of 200m flights (Table 3).

Tables 3 The ID Used to Indicate the Results from Difference Flights and Experiments

ID	Name
A001	CHM_50m_Point_Could_ZonalSta_100cm_buffer
A002	CHM_50m_Point_Could_ZonalSta_150cm_buffer
A003	CHM_50m_Point_Could_ZonalSta_200cm_buffer
A004	CHM_50m_Point_Could_ZonalSta_50cm_buffer
A005	CHM_50m_Point_Could_ZonalSta_no_buffer
A006	50m_cos_geo_CHM_ZonalSta_100cm_buffer
A007	50m_cos_geo_CHM_ZonalSta_150cm_buffer
A008	50m_cos_geo_CHM_ZonalSta_200cm_buffer
A009	50m_cos_geo_CHM_ZonalSta_50cm_buffer
A010	50m_cos_geo_CHM_ZonalSta_no_buffer
A011	50m_de_geo_CHM_ZonalSta_100cm_buffer
A012	50m_de_geo_CHM_ZonalSta_150cm_buffer
A013	50m_de_geo_CHM_ZonalSta_200cm_buffer
A014	50m_de_geo_CHM_ZonalSta_50cm_buffer
A015	50m_de_geo_CHM_ZonalSta_no_buffer
A016	50m_de_no_CHM_ZonalSta_100cm_buffer
A017	50m_de_no_CHM_ZonalSta_150cm_buffer
A018	50m_de_no_CHM_ZonalSta_200cm_buffer
A019	50m_de_no_CHM_ZonalSta_50cm_buffer
A020	50m_de_no_CHM_ZonalSta_no_buffer
A021	50m_cos_no_CHM_ZonalSta_100cm_buffer
A022	50m_cos_no_CHM_ZonalSta_150cm_buffer
A023	50m_cos_no_CHM_ZonalSta_200cm_buffer
A024	50m_cos_no_CHM_ZonalSta_50cm_buffer
A025	50m_cos_no_CHM_ZonalSta_no_buffer
B001	CHM_200m_Point_Could_ZonalSta_100cm_buffer
B002	CHM_200m_Point_Could_ZonalSta_150cm_buffer
B003	CHM_200m_Point_Could_ZonalSta_200cm_buffer
B004	CHM_200m_Point_Could_ZonalSta_50cm_buffer
B005	CHM_200m_Point_Could_ZonalSta_no_buffer
B006	200m_cos_geo_CHM_ZonalSta_100cm_buffer
B007	200m_cos_geo_CHM_ZonalSta_150cm_buffer
B008	200m_cos_geo_CHM_ZonalSta_200cm_buffer
B009	200m_cos_geo_CHM_ZonalSta_50cm_buffer
B010	200m_cos_geo_CHM_ZonalSta_no_buffer
B011	200m_de_geo_CHM_ZonalSta_100cm_buffer
B012	200m_de_geo_CHM_ZonalSta_150cm_buffer
B013	200m_de_geo_CHM_ZonalSta_200cm_buffer
B014	200m_de_geo_CHM_ZonalSta_50cm_buffer
B015	200m_de_geo_CHM_ZonalSta_no_buffer
B016	200m_de_no_CHM_ZonalSta_100cm_buffer
B017	200m_de_no_CHM_ZonalSta_150cm_buffer
B018	200m_de_no_CHM_ZonalSta_200cm_buffer

ID	Name
B019	200m_de_no_CHM_ZonalSta_50cm_buffer
B020	200m_de_no_CHM_ZonalSta_no_buffer
B021	200m_cos_no_CHM_ZonalSta_100cm_buffer
B022	200m_cos_no_CHM_ZonalSta_150cm_buffer
B023	200m_cos_no_CHM_ZonalSta_200cm_buffer
B024	200m_cos_no_CHM_ZonalSta_50cm_buffer
B025	200m_cos_no_CHM_ZonalSta_no_buffer

In table above, 50 and 200 represent 50m and 200m flight, CHM represent Tree Height, ZonalSta represent zonal statistic, cos represent customized settings, de represent default settings, geo represent georeferenced, no represent no buffer, no represent no georeferenced, and Point Cloud represent results from point cloud-classification.

Tables 4 Group CHM from Classification and Photogrammetry Produces

ID		Group CHM extractions
A001	B001	
A002	B002	
A003	B003	CHM from Point Could Classifications
A004	B004	
A005	B005	
A006	B006	
A007	B007	
A008	B008	CHM from Photogrammetry Products-Customized with georeferenced methods
A009	B009	
A010	B010	
A011	B011	
A012	B012	
A013	B013	CHM from Photogrammetry Products-Defaults with georeferenced methods
A014	B014	
A015	B015	
A016	B016	
A017	B017	
A018	B018	CHM from Photogrammetry Products-Defaults with no-georeferenced methods
A019	B019	
A020	B020	
A021	B021	
A022	B022	
A023	B023	CHM from Photogrammetry Products-customized with no-georeferenced methods
A024	B024	
A025	B025	

3.13 Statistical Analysis and Validation of Data

The most common methods to analyze statistically and validate height estimation and ground data are the root mean square error (RMSE), the coefficient determination (R^2), mean absolute error (MAE), bias, and the linear regression applied to present relationship of data (A. Birdal, 2016; Kameyama & Sugiura, 2020; L. Li et al., 2020; Panagiotidis et al., 2017; Peng et al., 2021; Zainuddin et al., 2016). In this study, descriptive statistic was used to indicate our field measures and height estimation. Liang et al. (2013) were applied minimum, maximum, mean, and standard deviation from descriptive statistics to present their field data collection. In addition, Y.-Q. Li et al. (2015) used descriptive statistics to indicate, calibrate and validate data. Box and whisker plots were used to summarize the descriptive statistics into four parts, 25% less than first quartile, 25% between first quartile (25 samples percentile) and second quartile (sample median or 50 sample percentile), 25% between second and third quartile (sample 75 percentile), and 25% larger than the third quartile (Ross, 2014). Panagiotidis et al. (2017) applied quartile to distribute the height estimate and field measurements into three parts: quartile 1 (25% lower), quartile 2 (50% or median), and quartile 3 (75%). Secondly, RMSE was calculated in equation 3. The relative value in % is given in equation 4. The Bias is shown in equation 5 with the relative Bias in % equation 6. The mean absolute error (MAE) to show the estimation errors and compare to field measurement (Equation 7). Y.-Q. Li et al. (2015) applied RMSE to assess the precision of estimation as the small RMSE indicated to be a better result. They used coefficient of determination to show the relationship of field measurements and estimations to show that higher value has strong a relationship and fit to ground data. Bias and relative bias were used in their research as well. The used statistic to assess the difference of two variables with respect to ground data. Third, a linear regression was calculated to indicate how the estimated result fit observation data. The residual indicates goodness of the fit in comparison with field data. Additionally, exploration data and visualizations were used to clarify outliers from estimates with field measurements by using orthophoto from photogrammetry products. Finally, the determination of the difference of field measurements and height estimates were done by application of paired sample t-test (Panagiotidis et al., 2017). This is used to identify

the difference of mean between two paired differ from 0 (Equation 8), which assess two hypothesis (A. Birdal, 2016):

- H_0: there is no significance difference between field measured and estimated height at 95% significance level. If (μ_1-μ_2=0).
- H_0: there is significance difference between field measured and estimated height at 95% significance level. If (μ_1-$\mu_2 \neq 0$).

$$RMSE = \sqrt{\frac{1}{n}\sum_{i=1}^{n}(h_{uav} - h_f)^2} \qquad (3)$$

$$RMSE\% = \frac{RMSE}{h} \times 100 \qquad (4)$$

$$Bias = \frac{1}{n}\sum_{i=1}^{n}(h_{uav} - h_f) \qquad (5)$$

$$Bias\% = \frac{Bias}{h} \times 100 \qquad (6)$$

$$MAE = \frac{1}{n}\sum_{i=1}^{n}|h_{uav} - h_f| \qquad (7)$$

$$t = \frac{d_f}{\sqrt{\frac{s^2}{n}}} \qquad (8)$$

Where h_{uav} is the measured height of UAV

h_f is height of field measurement

n is the number of trees

h is mean of height from field measurement n value

MAE is an mean of absolute errors

t is a paired t-test with n-1 degrees freedom

d_f is the difference by mean of two variables

s^2 is sample variance.

The statistical analysis were computed mostly in data analysis tools of Microsoft Excel. The input data for the linear regression is field measurements vs predicted values. The output are regression residuals (the difference between field measurement and prediction), residual plots and line fit (relationship between field measurement and prediction). In Excel, data analysis tools can be used to test the

hypothesis, t-test: paired two sample for means, t-test: two samples assuming equal variances, t-test: two samples assuming unequal variances, z-test: two samples for means, ztest, ttest (Harmon, 2011). In this study, a t-test of paired two samples for means were used. T-test tools (Figure 13) can be done by following method below:

- Variable 1: field measurement
- Variable 2: predict results
- Alpha: the level of significance $\alpha = 0.05$, p values < 0.05, two varriables significant difference

Figures 13 T-Test: Paired Two Sample for Means in Excel

CHAPTER 4
RESULT and DISCUSSION

4.1 Image Processed Analysis

The UAV images were processed separately with two tests. First, UAV images were analyzed with no GCPs marking in order to test onboard GPS compare to ground references and UAV images. Followed by two reprocessing steps in photogrammetry by adding and marking GCPs included checked points. GCPs design was 1.5 m x 1.5 m which was created as a center cross by spraying red color on the ground. 9 GCPs (Figure 14) were collected during field works, respectively to GCPs recommendation from Pix4d. Then 5 GCPs were used, 4 at the corner and 1 at the center. Others were used for checked points, and we used as 4 checked points. The absolute geolocation variance was good with no GCPs in both flights of 50 m and 200 m (Table 5) while RMSE contained less than 20 cm error in the geolocation error in X and Y direction, and about 50 cm for Z direction without GCPs marking for both flights. However, the performance of the GCPs marking was not very well. The RMSE was larger than 1 m in X and Y direction and in Z direction it varied between 2 to 5 m for both flights.
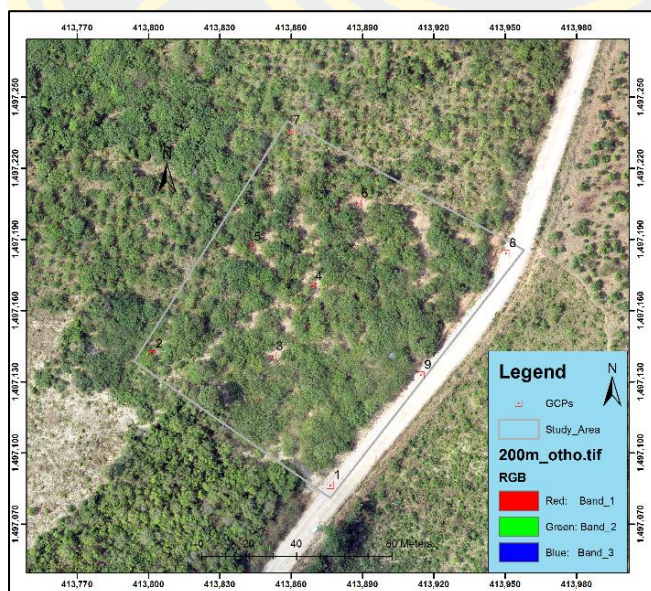
(a) 9 GCPs placements   (b) : GCPs design

Figures 14 GCPs Placement and Design

Tables 5 RMS Error in Images Processing from both 50m and 200m Flights

RMS error	X (m)	Y (m)	Z (m)	Notes
50m flight	0.180248	0.091116	0.508473	Without GPCs
	0.723803	1.396227	2.722710	With GCPs
200m flight	0.168268	0.258000	0.304005	Without GCPs
	1.496264	0.866824	5.434951	With GPCs

4.2 Tree Height Estimation

Ground truth data show that among 50 trees randomly selected the quartile median is 6.19 m while the maximum is 8.34 m and the minimum is 4.17 m. The estimations were similar to ground data for both flights based on point cloud classification. Most results were less than 1 m. However, the similar results of quartile from photogrammetric software of the 50 m flight are A011, A012, A013, A016, A017, A018, A019, and A020 with medians of 5.78 m, 5.83 m, 5.92 m, 5.37 m, 4.85 m, 5.78 m, 5.83 m, 5.92 m, 5.37 m, and 4.85 m. The minimum values were 3.09 m, 3.55 m, 3.68 m, 2.28 m, 0.01 m, 3.09 m, 3.55 m, 3.68 m, 2.28 m, and 0.01 m. The maximum values were 7.55 m, 9.89 m, 9.89 m, 6.79 m, 6.26 m, 7.55 m, 9.89 m, 9.89 m, 6.79 m, and 6.26 m (Table 6). In table 7, the results from the photogrammetric software of the 200 m flight are only B011, B012, B013, B016, B017, B018, and B023 which the median are 5.38 m, 5.71 m, 5.83 m, 5.38 m, 5.71 m, 5.83 m, and 4.61 m. The maximum values were 6.83 m, 6.98 m, 7.43 m, 6.83 m, 6.98 m, 7.43 m, and 6.28 m. The minimum values were 2.15 m, 2.15 m, 2.95 m, 2.15 m, 2.15 m, 2.95 m, and 2.05 m. Others contained predicted values larger than 1 m which means that compare to ground data, the results were lower.

Root mean square error (RMSE) indicates that the prediction errors were mostly less than 1 m for A001, A002, A003, A004, A005, B001, B002, B003, B004, B005, B011, B017, B018 and B019 were 0.60 m, 0.54 m, 0.56 m, 0.73 m, 1.13 m, 0.96 m, 0.80 m, 0.73 m, 1.21 m, 1.62 m, 1.13 m, 0.94 m, 0.81 m, and 1.33 m. Similarly, the bias were not much difference of prediction results and field measurement which the bias are -0.10, 0.03, 0.15, -0.33, -0.83, -0.64, -0.44, -0.28, -0.96, -1.37, -0.80, -0.58, -0.41, and -1.00. In addition, MAE were 0.10, 0.03, 0.15, 0.33, 0.83, 0.64, 0.44, 0.28, 0.96, 1.37, 0.80, 0.58, 0.41, and 1.00. It was shown that A006, A007, A008, A009, A010, A021, A022, A023, A024, and A025 are similar to B006, B007, B008, B009,

B010, B012, B013, B014, B015, B016, B020, B021, B022, B023, B024, and B025. They show high RMSE, bias, and MAE ranges from 3.50 m to 4.50 m, -3.57 m to -0.32 m, and 0.32 m to 3.57 m prediction errors (Table 8).

Box and whisker indicated that the predicted results of A001 to A005, B01 to B05, and B011, B016, B017, B018, B019 were similar to the estimated results. In comparison to field measurements, the field median result was 6.19 m while the predicted results were 6.74 m, 6.83 m, 6.93 m, 6.58 m, 5.98 m, 5.55 m, 5.75 m, 5.80 m, 5.19 m, 4.84 m, 5.38 m, 5.38 m, 5.71 m, 5.83 m, and 5.32 m. The others estimations were extremely low compared to ground data, for example, the estimates of A020 to A025 were 4.85, 2.70, 3.02, 3.40, 2.37, and 2.01 (Figure 15).

Radius plots show that A001, A002, A003, A004, B001, B002, B003, B004, B011, B012, B013, B017, and B018 contained a lower prediction error compared to field data which range from 1 to -1 and MAE were 0.10, 0.03, 0.15, 0.33, 0.64, 0.44, 0.28, 0.96, 0.80, 0.58, 0.58, and 0.41. Mostly, other predictions were underestimated with a MAE larger than 1 m to less than 3.57.

The regression indicates that A001 has a medium relationship. R^2 was 0.55. A002 and A003 had similar results 0.60. A004 and A005 had a low relationship from 0.49 and 0.40 (Figure 16). The data from the 200 m flight show that the R^2 range from 0.40 to 0.45 with B001, B002, B003, B005, B011, B017, B018, and B019. B004 shows the highest R^2 value of 0.49 (Figure 17). The best results of height estimation of both flights are A002 and B004 with RMSE, MAE, R^2 of 0.54, 0.03, 0.60 and 1.21, 0.96, 0.48.

Tables 6 Descriptive Statistic Summarized of Tree Height Estimations and Reference Data from 50m Flight

-	Q0	Q1	Q2	Q3	Q4
Ref	**4.17**	**5.65**	**6.19**	**6.97**	**8.34**
A001	4.18	5.52	6.16	6.74	7.90
A002	4.37	5.58	6.17	6.83	7.90
A003	4.63	5.62	6.24	6.93	8.07
A004	3.45	5.33	6.02	6.58	7.41
A005	2.19	4.93	5.51	5.98	6.78
A006	0.02	1.25	2.70	4.05	6.04
A007	0.12	1.65	3.02	4.39	6.13
A008	0.15	2.16	3.40	4.48	6.13

-	Q0	Q1	Q2	Q3	Q4
Ref	**4.17**	**5.65**	**6.19**	**6.97**	**8.34**
A009	0.02	0.71	2.37	3.92	5.76
A010	0.00	0.45	2.01	3.72	5.45
A011	3.09	5.07	5.78	6.06	7.55
A012	3.55	5.15	5.83	6.30	9.89
A013	3.68	5.19	5.92	6.30	9.89
A014	2.28	4.80	5.37	5.91	6.79
A015	0.01	4.05	4.85	5.55	6.26
A016	3.09	5.07	5.78	6.06	7.55
A017	3.55	5.15	5.83	6.30	9.89
A018	3.68	5.19	5.92	6.30	9.89
A019	2.28	4.80	5.37	5.91	6.79
A020	0.01	4.05	4.85	5.55	6.26
A021	0.02	1.25	2.70	4.05	6.04
A022	0.12	1.65	3.02	4.39	6.13
A023	0.15	2.16	3.40	4.48	6.13
A024	0.02	0.71	2.37	3.92	5.76
A025	0.00	0.45	2.01	3.72	5.45

In the table: Ref is reference data or field measured and Q is quartiles (Q0: minimum value, Q1: 25% (lower), Q2: 50% (median), Q3: 25% (upper), and Q4: maximum value).

Tables 7 Descriptive Statistic Summarized of Tree Height Estimations and Reference Data from 200m Flight

-	Q0	Q1	Q2	Q3	Q4
Ref	**4.17**	**5.65**	**6.19**	**6.97**	**8.34**
B001	2.98	5.04	5.55	6.14	6.96
B002	3.99	5.17	5.75	6.25	7.36
B003	3.99	5.38	5.80	6.65	7.44
B004	2.24	4.74	5.19	5.96	6.71
B005	1.87	4.23	4.84	5.59	6.61
B006	1.58	3.53	4.36	4.77	6.03
B007	1.82	3.81	4.48	4.94	6.25
B008	2.05	3.90	4.61	5.20	6.28
B009	1.42	2.92	4.08	4.60	5.79
B010	0.01	2.40	3.74	4.37	5.58
B011	2.15	4.96	5.38	6.06	6.83
B012	2.15	5.03	5.71	6.23	6.98
B013	2.95	5.16	5.83	6.36	7.43
B014	1.23	4.70	5.32	5.96	6.58
B015	1.21	4.34	5.01	5.76	6.46
B016	2.15	4.96	5.38	6.06	6.83

-	Q0	Q1	Q2	Q3	Q4
Ref	**4.17**	**5.65**	**6.19**	**6.97**	**8.34**
B017	2.15	5.03	5.71	6.23	6.98
B018	2.95	5.16	5.83	6.36	7.43
B019	1.23	4.70	5.32	5.96	6.58
B020	1.21	4.34	5.01	5.76	6.46
B021	1.58	3.53	4.36	4.77	6.03
B022	1.82	3.81	4.48	4.94	6.25
B023	2.05	3.90	4.61	5.20	6.28
B024	1.42	2.92	4.08	4.60	5.79
B025	0.01	2.40	3.74	4.37	5.58

In the table: Ref is reference data or field measured and Q is quartiles (Q0: minimum value, Q1: 25% (lower), Q2: 50% (median), Q3: 25% (upper), and Q4: maximum value).

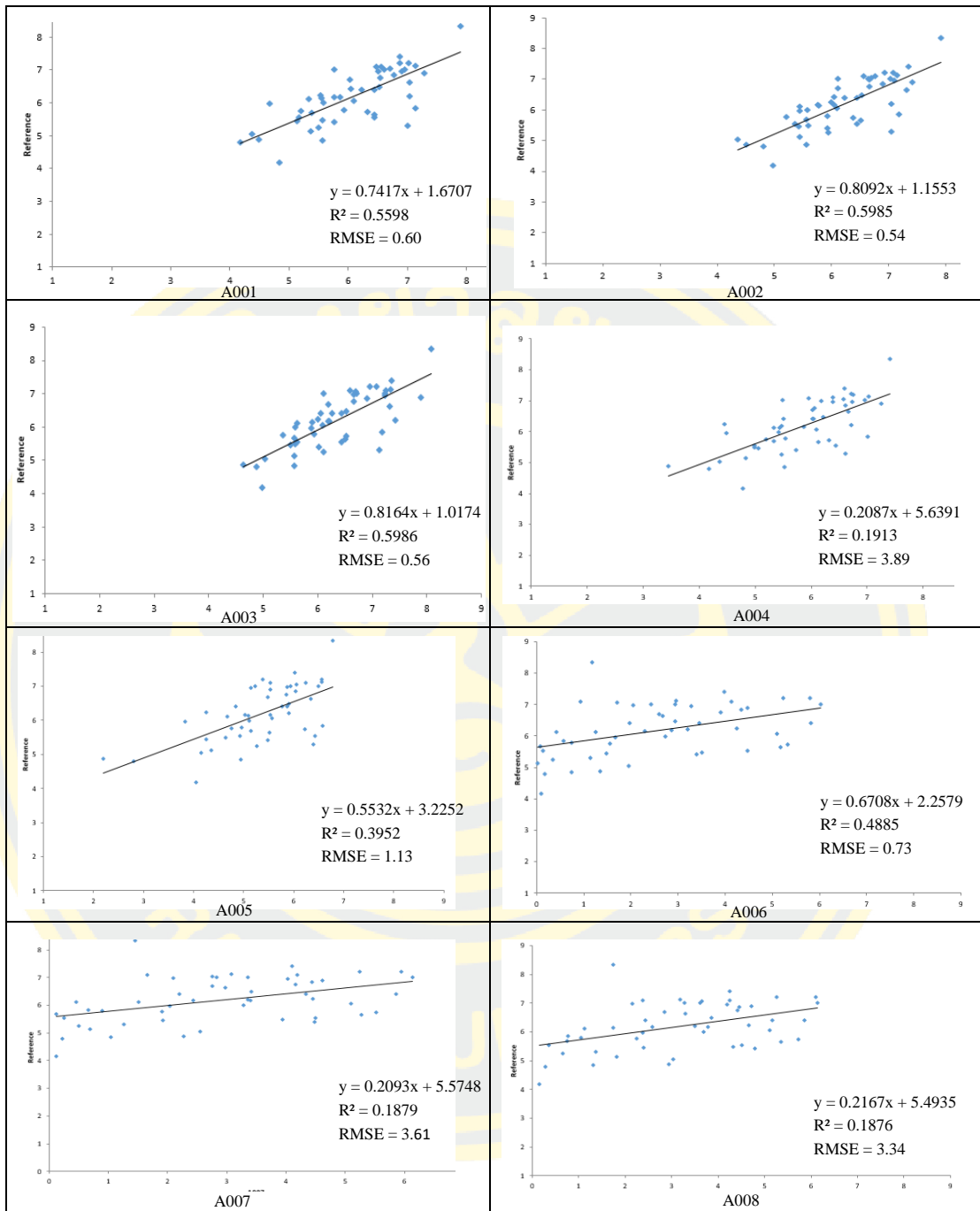Tables 8 The Estimation and Ground Truth from Both 50m Flight and 200m Flight

-	Bias	Bias (%)	RMSE(m)	RMSE (%)	MAE(m)	R^2
A001	-0.10	-1.59	0.60	9.64	0.10	0.5598
A002	0.03	0.50	0.54	8.81	0.03	0.5985
A003	0.15	2.35	0.56	9.07	0.15	0.5986
A004	-0.33	-5.34	0.73	11.85	0.33	0.4885
A005	-0.83	-13.48	1.13	18.31	0.83	0.3952
A006	-3.57	-57.67	3.89	62.92	3.57	0.1913
A007	-3.27	-52.83	3.61	58.42	3.27	0.1879
A008	-2.99	-48.35	3.34	54.03	2.99	0.1876
A009	-3.84	-62.14	4.15	67.15	3.84	0.1946
A010	-4.13	-66.69	4.41	71.21	4.13	0.2006
A011	-0.67	-10.77	1.17	18.99	0.67	0.1387
A012	-0.44	-7.13	1.16	18.72	0.44	0.122
A013	-0.32	-5.24	1.10	17.80	0.32	0.1096
A014	-0.97	-15.65	1.39	22.39	0.97	0.1384
A015	-1.51	-24.37	1.89	30.48	1.51	0.1455
A016	-0.67	-10.77	1.17	18.99	0.67	0.1455
A017	-0.44	-7.13	1.16	18.72	0.44	0.122
A018	-0.32	-5.24	1.10	17.80	0.32	0.1096
A019	-0.97	-15.65	1.39	22.39	0.97	0.1384
A020	-1.51	-24.37	1.89	30.48	1.51	0.1455
A021	-3.57	-57.67	3.89	62.92	3.57	0.1913
A022	-3.27	-52.83	3.61	58.42	3.27	0.1879
A023	-2.99	-48.35	3.34	54.03	2.99	0.1876
A024	-3.84	-62.14	4.15	67.15	3.84	0.1946

| -	Bias	Bias (%)	RMSE(m)	RMSE (%)	MAE(m)	R^2
A025	-4.13	-66.69	4.41	71.21	4.13	0.2006
B001	-0.64	-10.37	0.96	15.46	0.64	0.4392
B002	-0.44	-7.15	0.80	12.87	0.44	0.4465
B003	-0.28	-4.52	0.73	11.80	0.28	0.4327
B004	-0.96	-15.58	1.21	19.51	0.96	0.4852
B005	-1.37	-22.11	1.62	26.19	1.37	0.4169
B006	-2.04	-33.02	2.35	37.95	2.04	0.0808
B007	-1.86	-30.03	2.19	35.37	1.86	0.0565
B008	-1.71	-27.68	2.06	33.28	1.71	0.0615
B009	-2.34	-37.81	2.60	42.11	2.34	0.1946
B010	-2.80	-45.28	3.09	49.90	2.80	0.1815
B011	-0.80	-12.91	1.13	18.20	0.80	0.4144
B012	-0.58	-9.37	0.94	15.23	0.58	0.122
B013	-0.41	-6.70	0.81	13.13	0.41	0.1096
B014	-1.00	-16.20	1.33	21.55	1.00	0.1384
B015	-1.30	-20.94	1.67	26.96	1.30	0.3735
B016	-0.79	-12.85	1.13	18.24	0.79	0.1455
B017	-0.58	-9.37	0.94	15.23	0.58	0.416
B018	-0.41	-6.70	0.81	13.13	0.41	0.4377
B019	-1.00	-16.20	1.33	21.55	1.00	0.4009
B020	-1.30	-20.94	1.67	26.96	1.30	0.1455
B021	-2.04	-33.02	2.35	37.95	2.04	0.0808
B022	-1.86	-30.03	2.19	35.37	1.86	0.0565
B023	-1.71	-27.68	2.06	33.28	1.71	0.0615
B024	-2.34	-37.81	2.60	42.11	2.34	0.1311
B025	-2.80	-45.28	3.09	49.90	2.80	0.1815

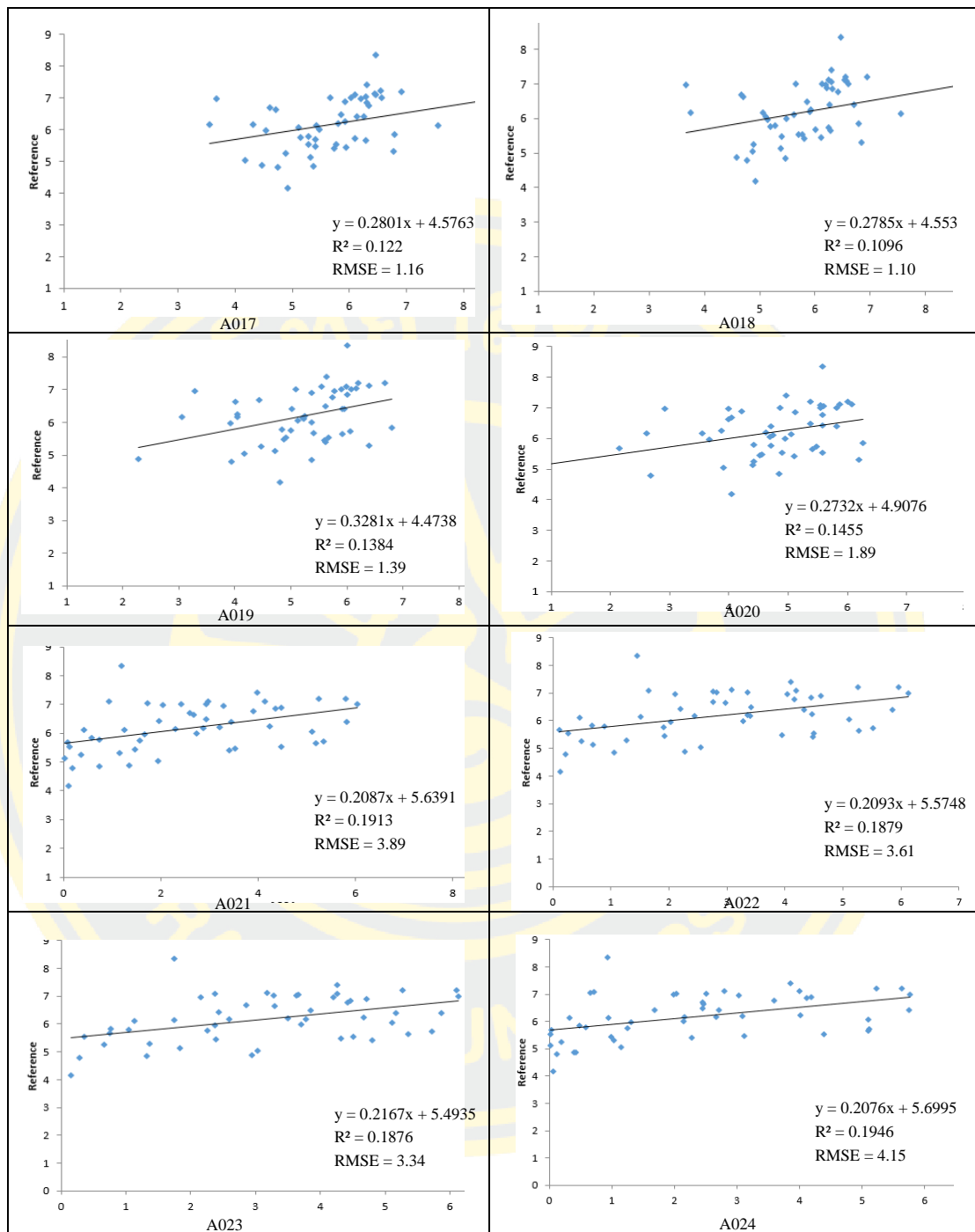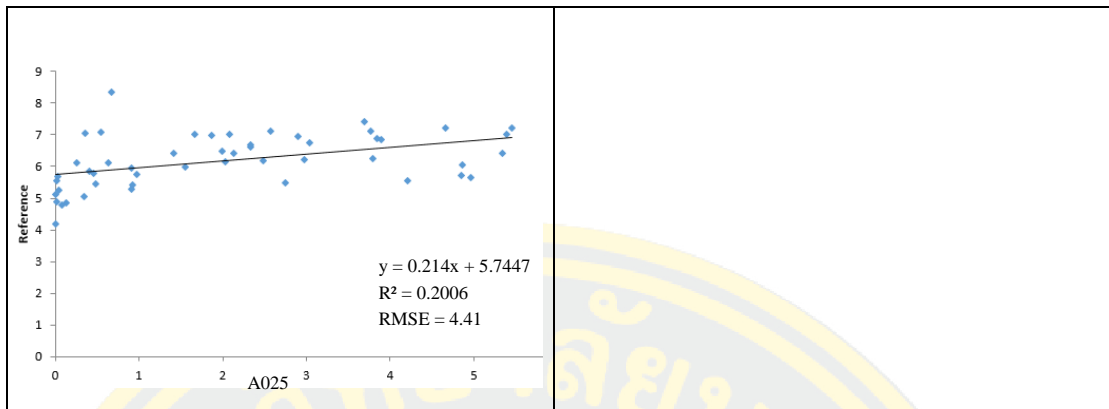Figures 15 Box Whisker Plot of the Estimation and Ground Truth from Both 50m Flight and 200m Flight

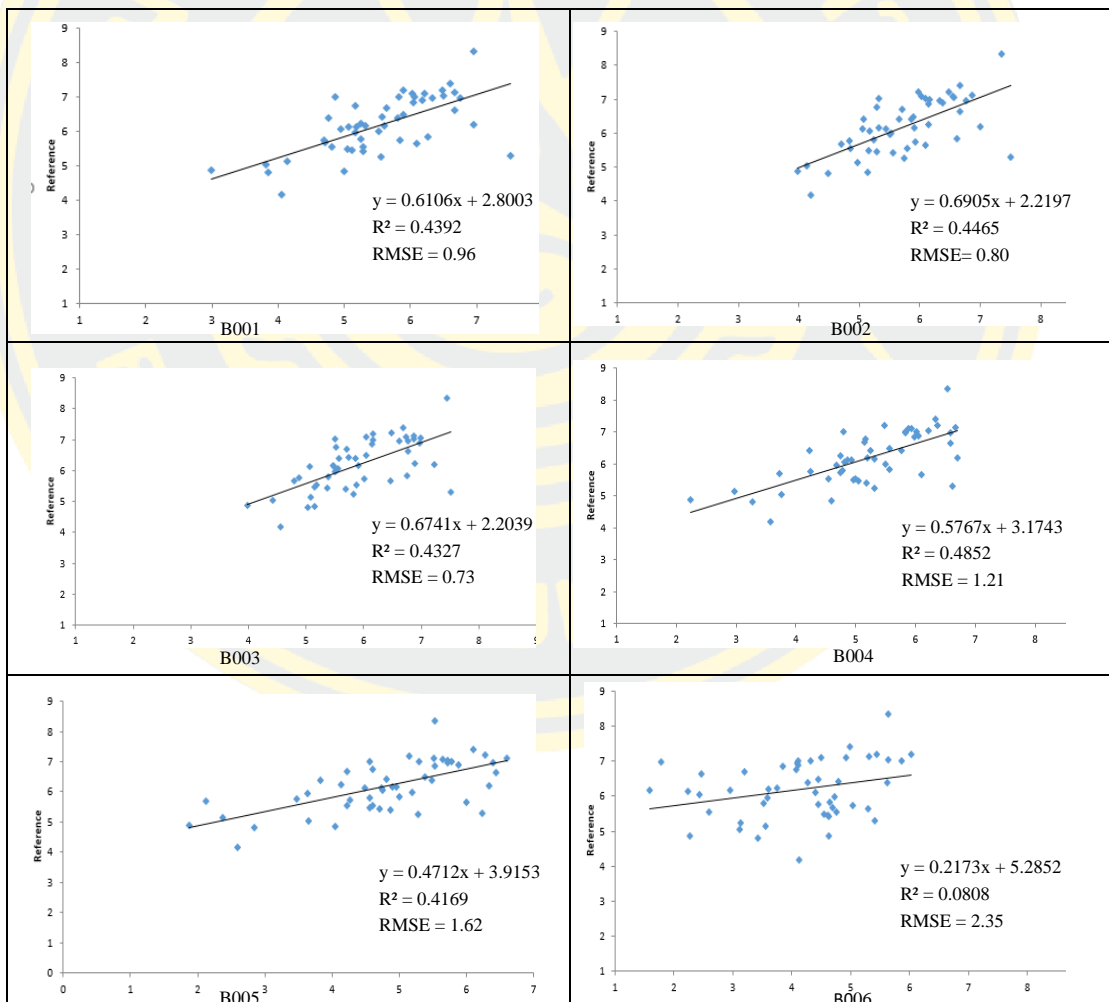Figures 16 Linear Regression Model of the Estimation and Ground Truth from 50m Flight
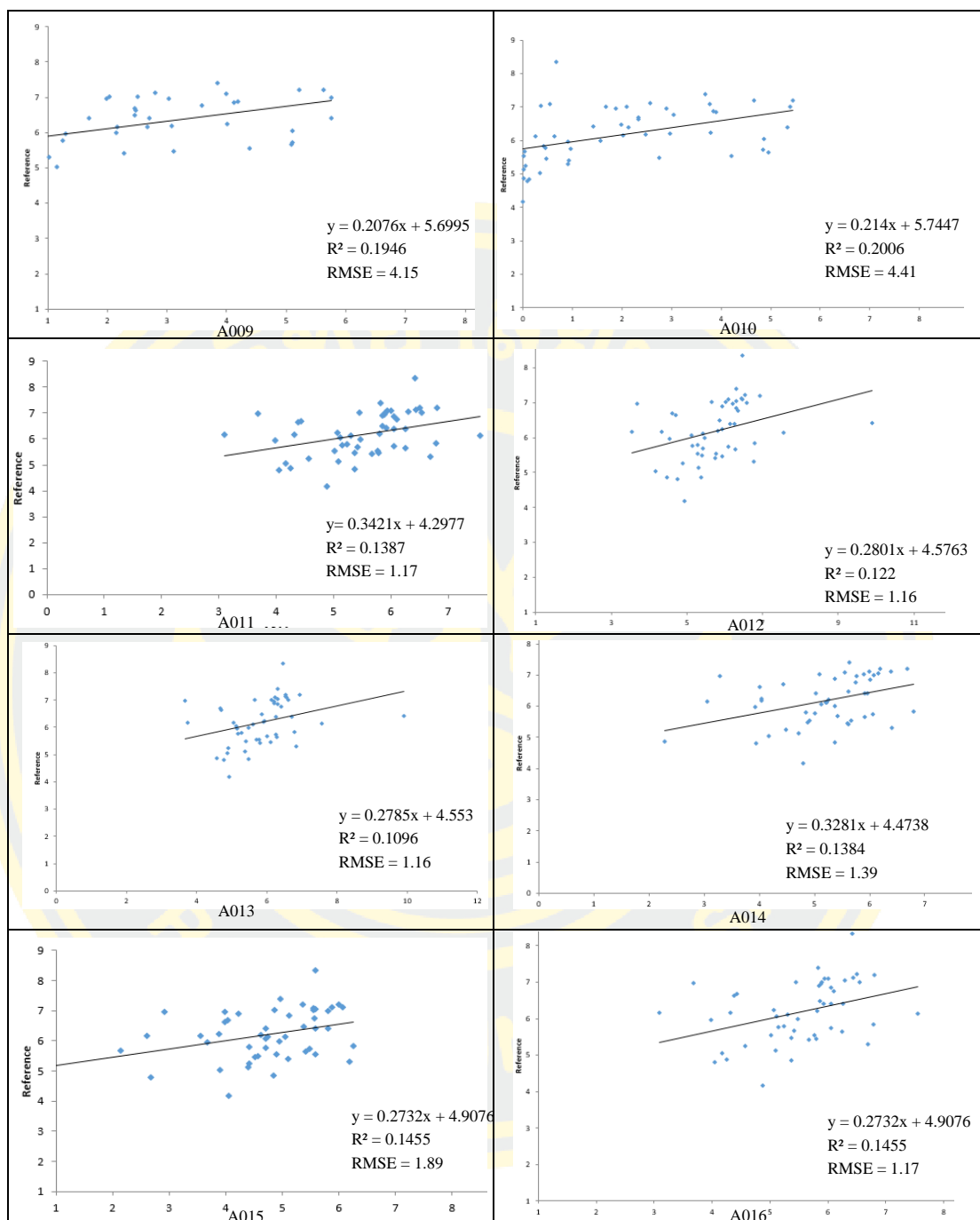
Figures 17 Linear Regression Model of the Estimation and Ground Truth from 50m Flight (cont.)
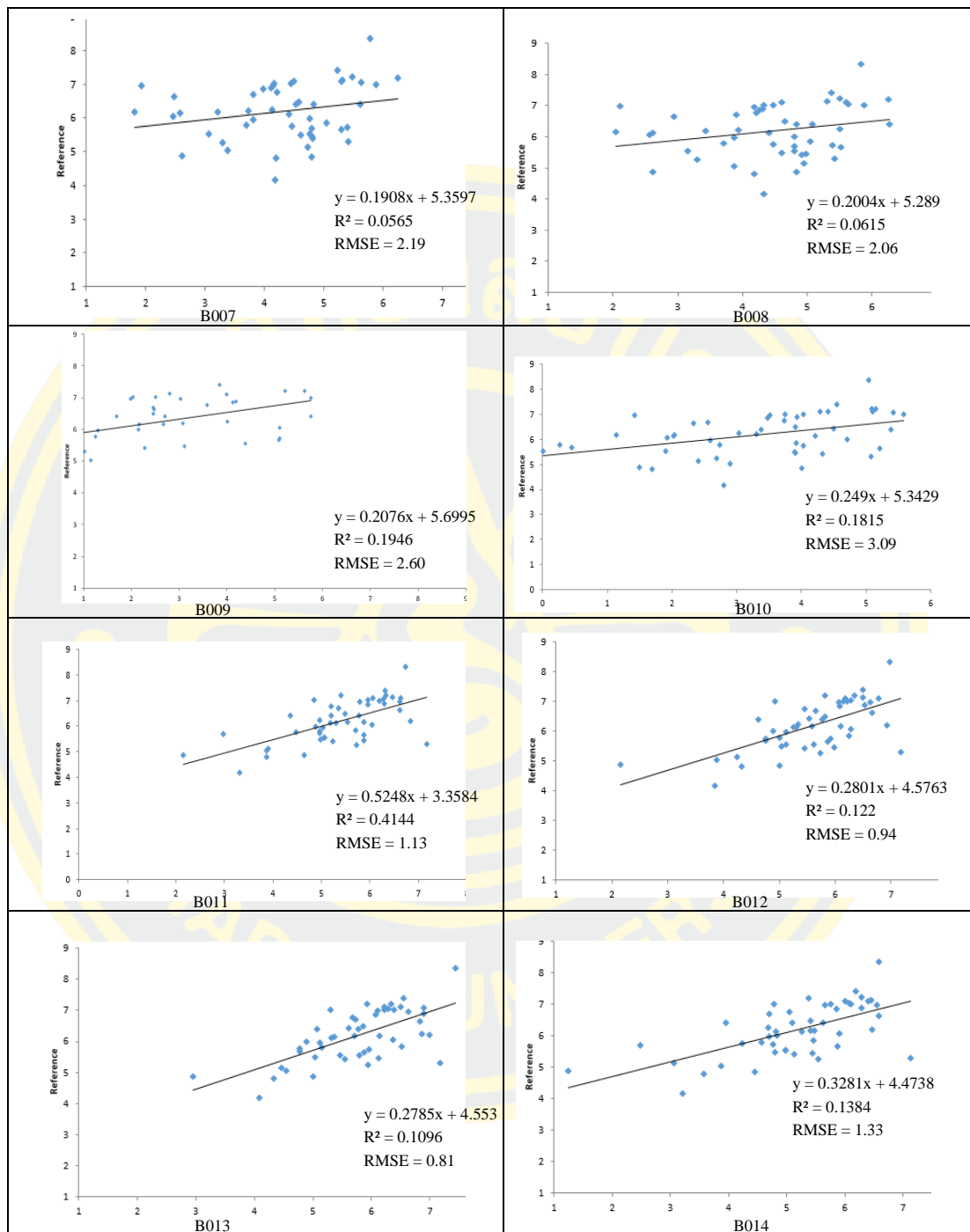
Figures 18 Linear Regression Model of the Estimation and Ground Truth from 50m Flight (cont.)
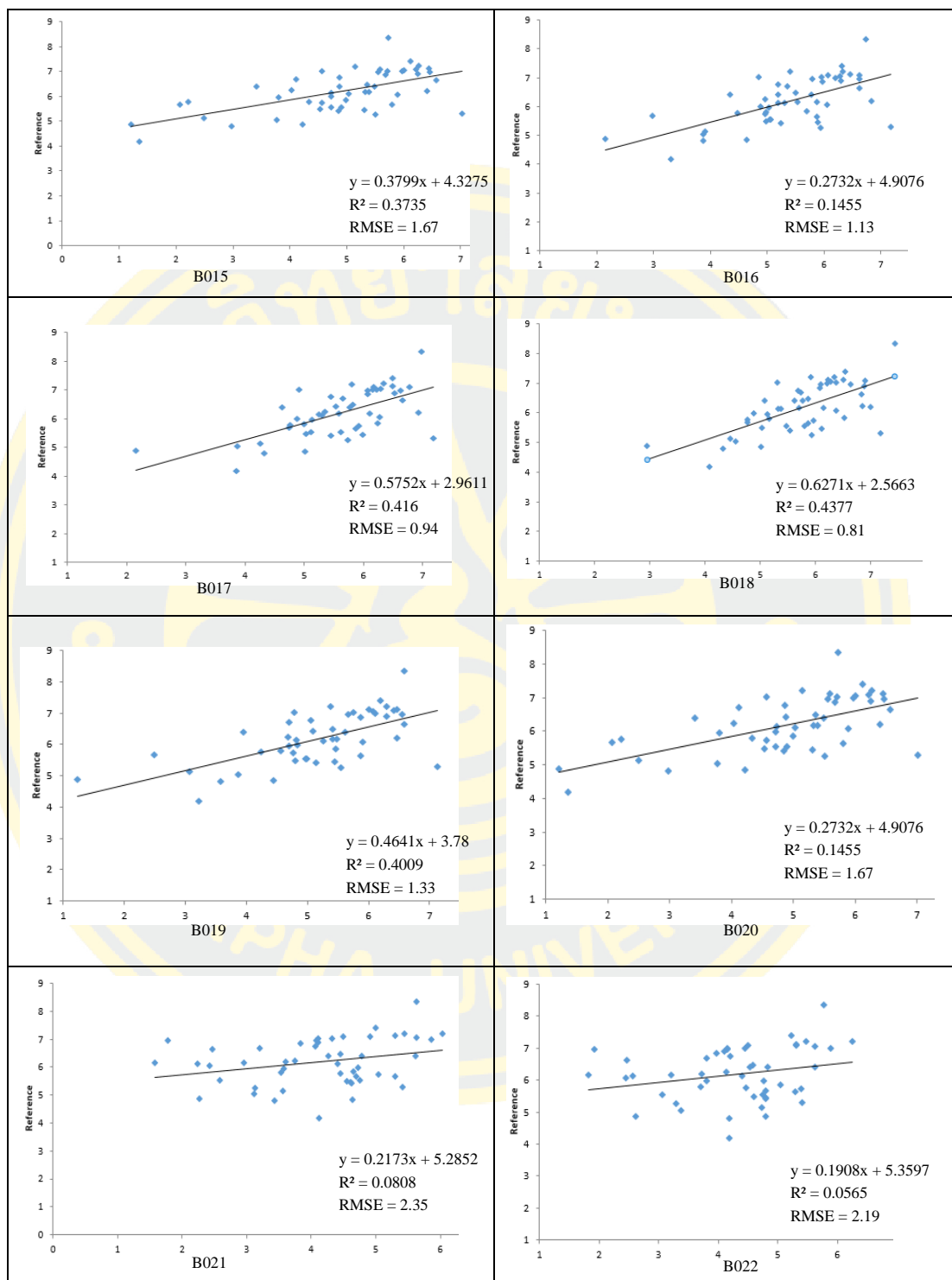
Figures 19 Linear Regression Model of the Estimation and Ground Truth from 50m Flight (cont.)
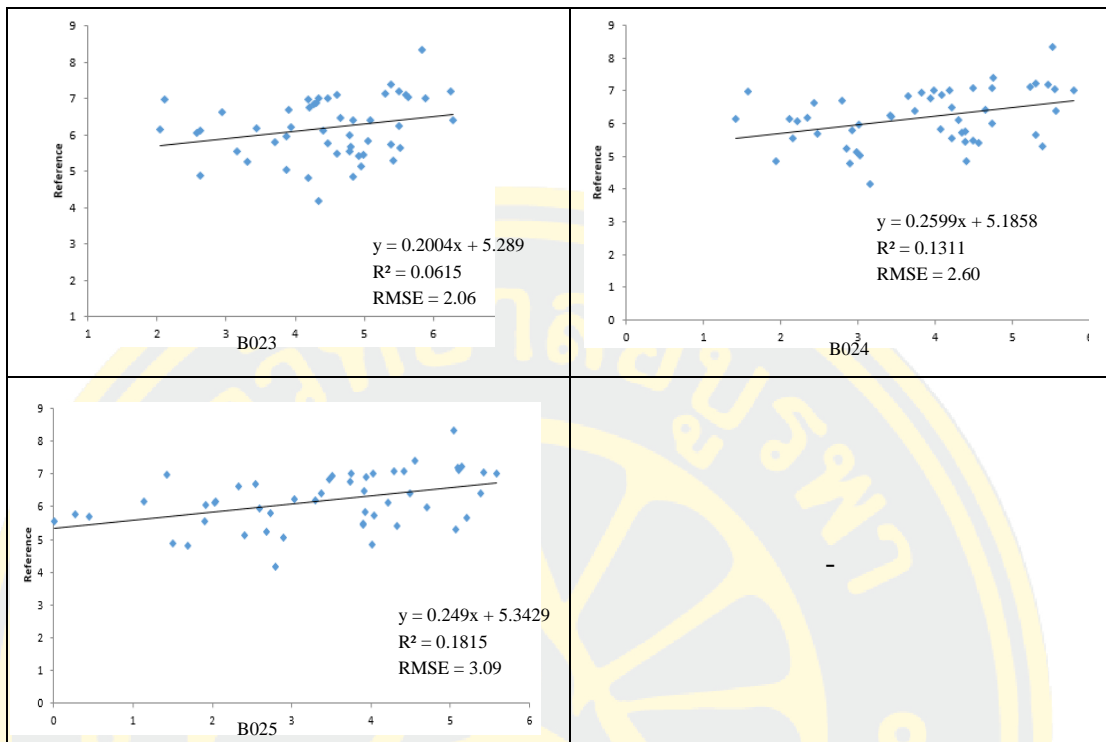

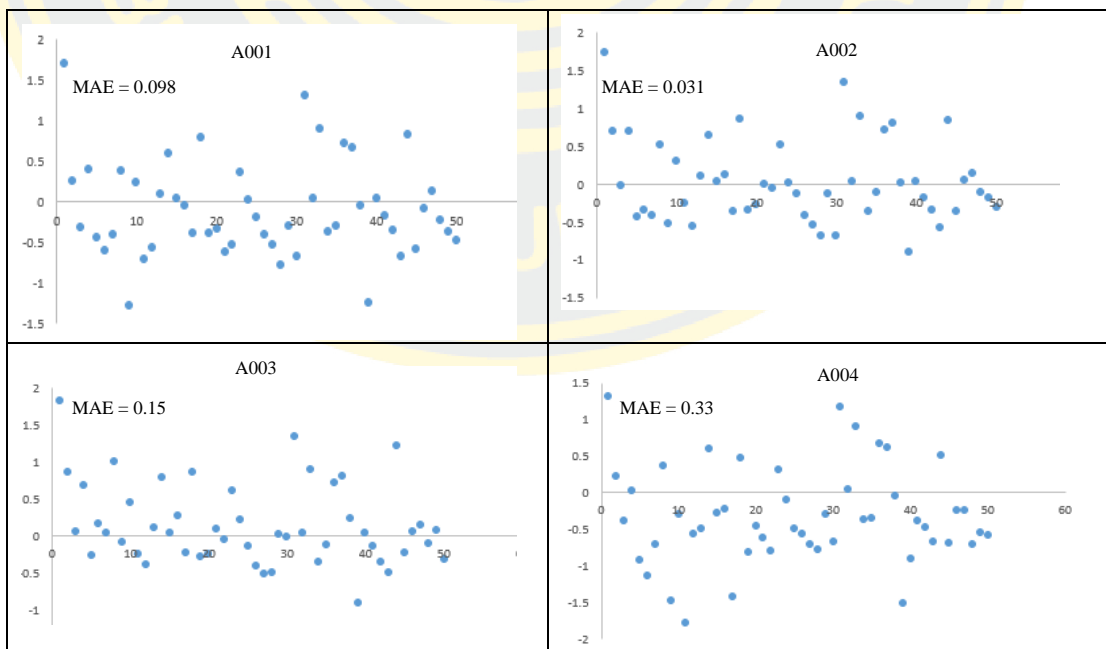Figures 20 Linear Regression Model of the Estimation and Ground Truth from 200m Flight

Figures 21 Linear Regression Model of the Estimation and Ground Truth from 200m Flight (cont.)

Figures 22 Linear Regression Model of the Estimation and Ground Truth from 200m Flight (cont.)

Figures 23 Linear Regression Model of the Estimation and Ground Truth from 200m Flight (cont.)

Figures 24 Residual Plots of the Estimation and Ground Truth from 50m Flight

Figures 25 Residual Plots of the Estimation and Ground Truth from 50m Flight (cont.)

Figures 26 Residual Plots of the Estimation and Ground Truth from 50m Flight (cont.)

Figures 27 Residual Plots of the Estimation and Ground Truth from 50m Flight (cont.)

Figures 28 Residual Plots of the Estimation and Ground Truth from 200m Flight

Figures 29 Residual Plots of the Estimation and Ground Truth from 200m Flight (cont.)

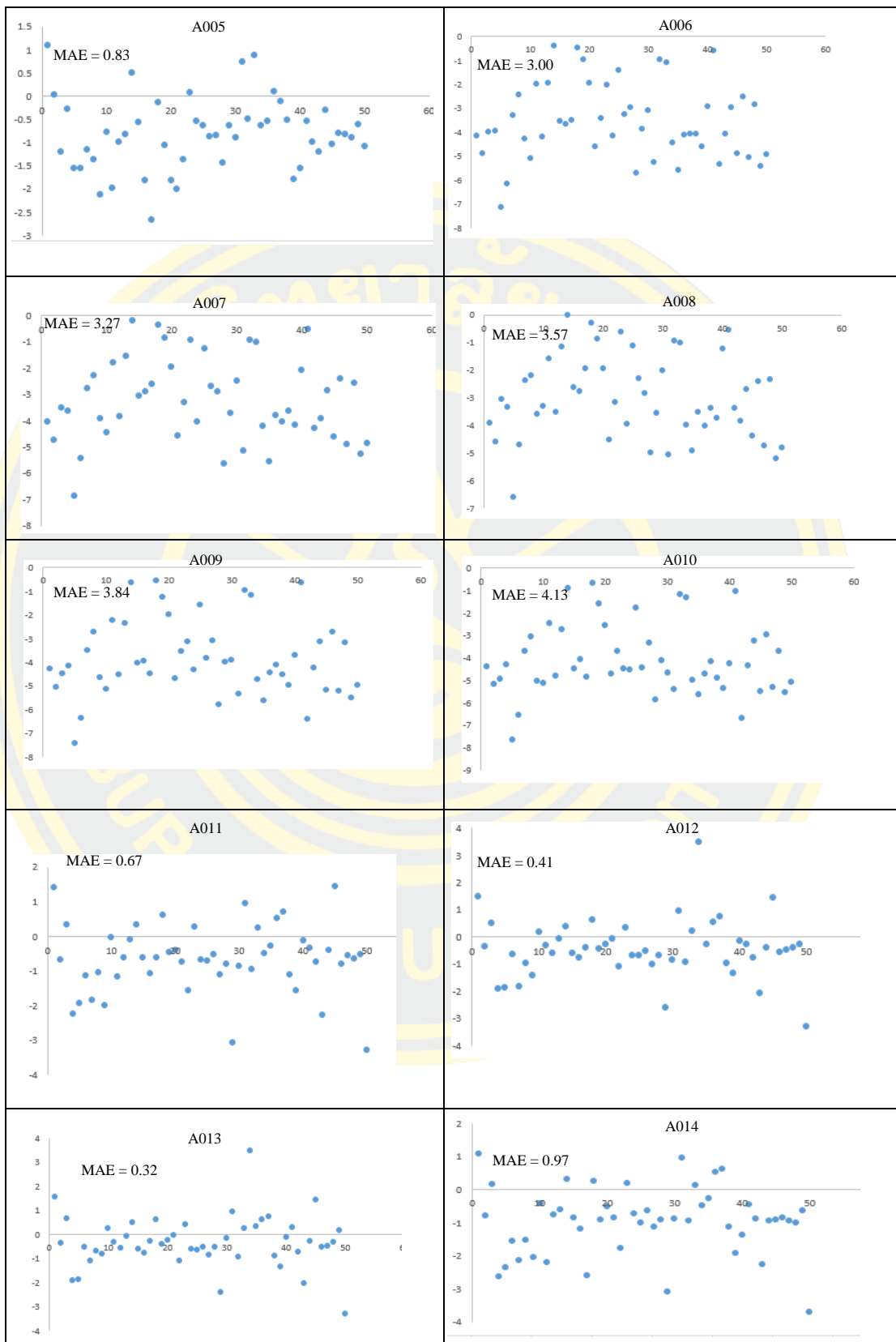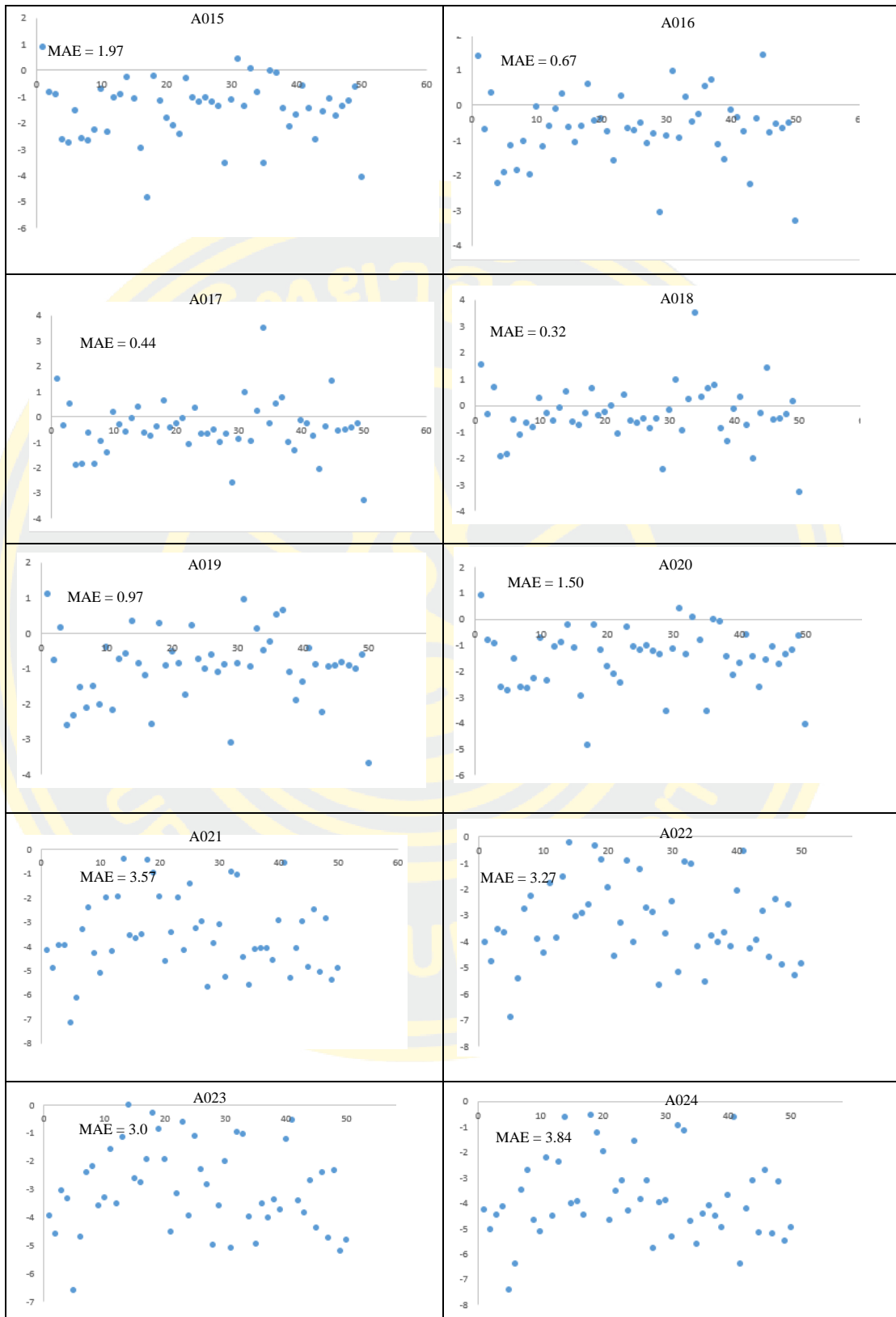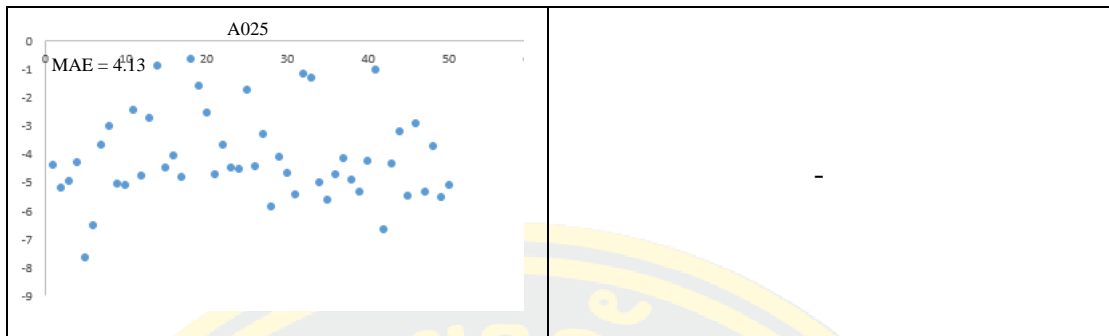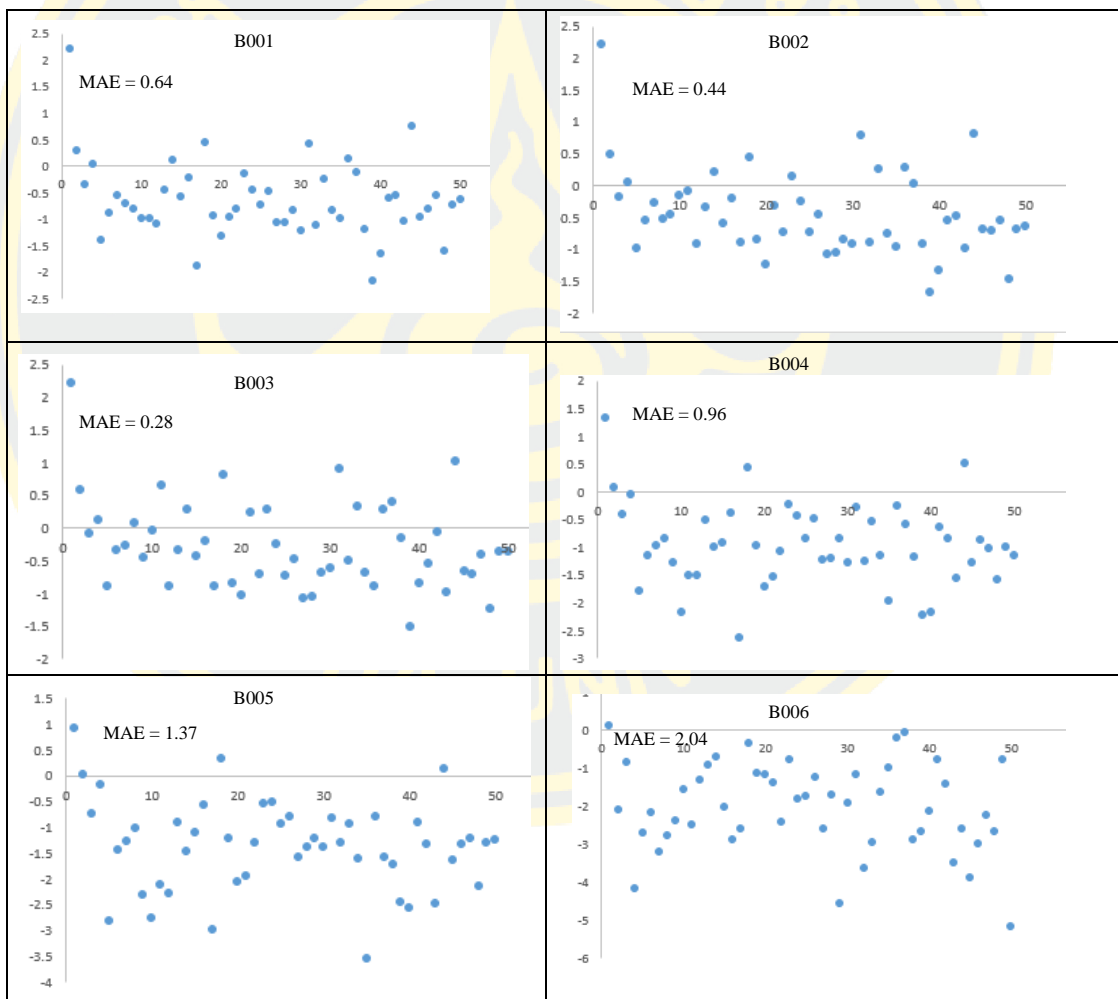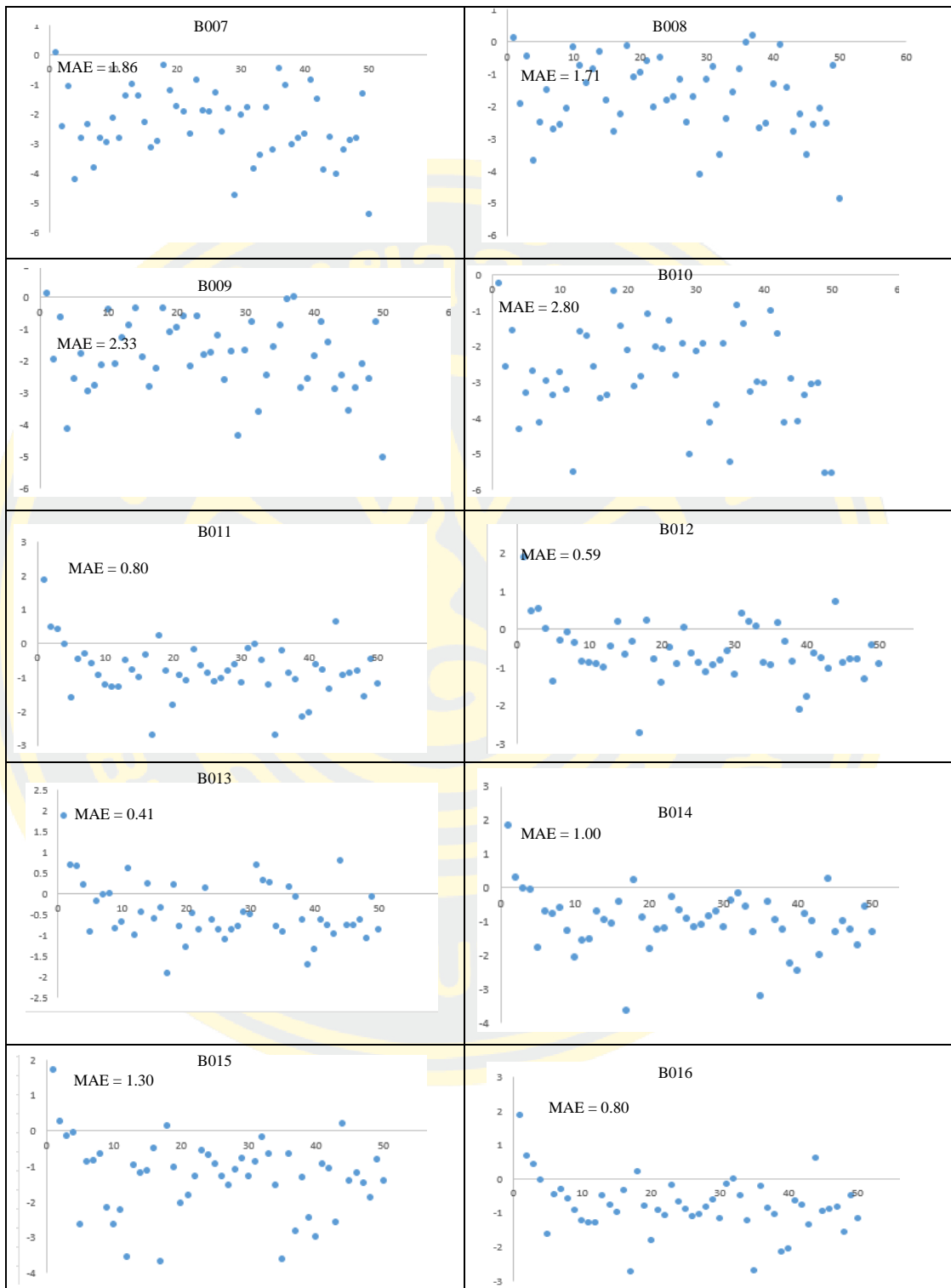Figures 30 Residual Plots of the Estimation and Ground Truth from 200m Flight (cont.)

4.3 Significance Difference of Tree Height Estimation

A001, A002, A003, A004, and A005 for 50m flight and B001, B002, B003, B004, B005, B011, B017, B018, and B019 were selected to compare in t-test as follow:

- Tree height estimated with ground data
- Tree height estimated with tree height estimated

The result shows that P values larger than 0.05, can't be rejected from the hypothesis of paired reference data with A001, A002, A003, and B019 and B004. However, P values less than 0.05, can be rejected from the hypothesis of reference data with A004, A005, B001, B002, B003, B004, B005, B011, B018, B019, and B018 and B003, B019 and A004, B011 and A001, B017 and A002, B018 and A003, B001 and A001, B002 and A002, B003 and A003, B004 and A004, B011 and B001, B017 and B002, B005 and A005.

Tables 9 Sample Paired T-Test of Tree Height Estimation and Ground Data

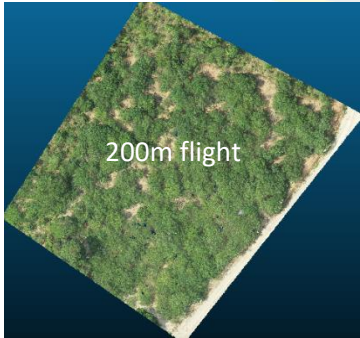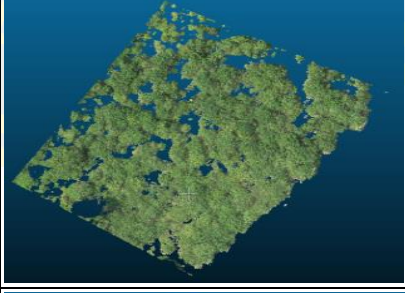| Significance	$P(T \leq t)$ two tail t test	t critical two tail t test	t start	df
Ref and A001	0.25	2.01	1.170	49
Ref and A002	0.70	2.01	-0.40	49
Ref and A003	0.07	2.01	-1.87	49
Ref and A004	0.00	2.01	3.54	49
Ref and A005	0.00	2.01	7.62	49
Ref and B001	0.00	2.01	6.33	49
Ref and B002	0.00	2.01	4.67	49
Ref and B003	0.00	2.01	2.89	49
Ref and B004	0.00	2.01	9.27	49
Ref and B005	0.00	2.01	11.02	49
Ref and B011	0.00	2.01	7.04	49
Ref and B017	0.00	2.01	5.46	49
Ref and B018	0.00	2.01	4.15	49
Ref and B019	0.00	2.01	7.99	49
B019 and B004	0.45	2.01	-0.77	49
B011 and B001	0.01	2.01	-2.63	49
B017 and B002	0.02	2.01	-2.42	49
B018 and B003	0.00	2.01	-2.79	49
B019 and A004	0.00	2.01	-6.89	49
B011 and A001	0.00	2.01	-7.64	49
B017 and A002	0.00	2.01	-8.81	49
B018 and A003	0.00	2.01	-9.34	49
B001 and A001	0.00	2.01	-8.59	49
B002 and A002	0.00	2.01	-9.46	49
B003 and A003	0.00	2.01	-8.87	49
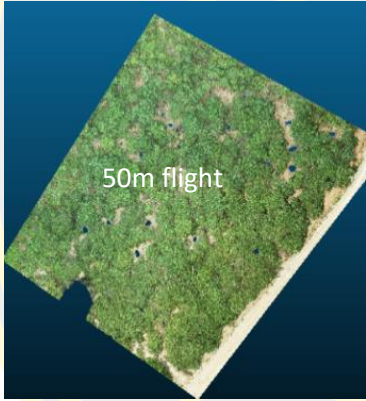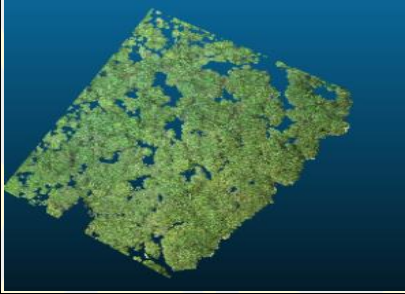
4.4 Uncertainty of Tree Height Estimation

In the present study, the height estimation was not well distributed. Very low accuracy of height estimation was achieved by photogrammetry products. The consequence is a huge bias and big error. This is caused by field data collector, the equipment uses, the effect of weather, methods applied in both data collection and data processing.

Tables 10 Uncertainty Tree Height Estimation

Types errors	How we used	limitation	solutions
Design height meters	We used pipe and cut it into many parts. But we have to make sure, it is removable fast and easy.	During measurement, it not similar with original meters, it sometimes curves.	We tried to place near to tree measured to make sure it not curves too much.
Design GCPs	We spay on the red color on ground. 1.5 x 1.5	Take 2 hours to design 9 GCPs	We tried to plan GCPs placements before go to field.
Field measurement	We used two persons, one respond for place the design meters at center of tree and hold it to top of tree	Some dense tree difficult to see top	Need to find suitable angle to see
Tree location	We placed emlid at the tree stump.	Cashew are not straight stand trees.	We assume the tree location is tree stump
Tree crown	-	Some of tree crown overlap with others trees.	-
UAVs	Auto capturing function: iso, sutter speed,	Image quality effect during capturing	-
Bad weather	We met cloudy situation	UAVs setting is complicated	Wait until weather better, but impossible
Small plant	-	Effect to point cloud density	-

Types errors	How we used	limitation	solutions
Photogrammetry used	Explore setting	Our computer very low specification	Try cloud processing
DTM and DSM settings	Change both flight to 5.48cm/pix	Effect to photogrammetry output	Classify point cloud
CFS filtering	Classify ground and none ground	Low vegetation not well class	Assign point clouds
Resampling	Change to 10cm	Effect to results	-

Sources	How we do?	Bias
50m flight		
200m flight		

Sources	How we do?	Bias
orthophoto		Field measure =5.3m Estimation =7m
		Field measure =7m Estimation =5m

Figures 31 Individual Tree Height Bias Exploration

4.5 Discussion

In the previous studies, various method has been applied to estimate tree heights from low-cost UAV with different camera and different sensors. Most previous research indicated results based on R^2, Linear regression model, RMSE, and Bias (Lussem, Schellberg, & Bareth, 2020; Paneque-Gálvez et al., 2014; Zainuddin et al., 2016). In our study, the GCPs designed showed that a RMSE of 1 cm is possible to get high accuracy for alignment of our images. However, there were several factors effected the obtained UAVs image quality, e.g., the bad weather condition. It was noticed that huge clouds moved around our study area during field data collection. The images were partly grayish covered (cloud block) during the 50 m flight. The 200 m flight produced better imagery. As a consequence, the applied GCPs show low accuracy which resulted from less light on the ground caused by tree crown cover, capture angles, and placement of GPCs. Instead of it, no GCPs were used in the resulted images to generate CHM, hence, another geo-referenced CHM was used for comparison. In this study, tree heights were generated from two sources, one from photogrammetry

software and one from semi-automatic point cloud classification. The resampling method was applied with high resolutions of 10 cm. The image processing was divided into different steps for both flights, 50 m, and 200 m, to test which setting should be used for tree height extraction and CHM from low-cost UAV to determine the height of cashew trees.

CHM extractions were divided into 5 groups. The first group relied CHM extraction from point cloud classification which was represented in different settings used in A001 to A005 and B001 to B005. Second group consisted of CHM extraction from photogrammetry with customized set up and with georeferenced which is shown in A006 to A010 and B006 to B010. Third group was based on CHM extraction from photogrammetry with defaults settings and geo-reference. It is represented in A011 to A015 and B011 to B015. Fourth group used CHM extraction from photogrammetry with defaults settings and no-georeferenced. It is given in A016 to A020 and B015 to B020. Fifth group was based on CHM extraction from photogrammetry with customized settings and no-georeferenced settings, A021 to A025 and B021 to B025. The results show that photogrammetry products indicated variations of 1 m for the tree. Among 40 differences were shown in the results based on different settings. In total 4 setting was acceptable from the 200 m flight, B011, B017, B018, and B019. The R^2 range was from 0.40 to 0.44. However, semi-automatic point cloud classification provides better results with R^2 range of 0.40 to 0.60. The highest R^2 value of the 200 m flight is 0.49. It was noticed that 50 m flight provides better point clouds. It contained cleaner values than the 200 m flight. In comparison with a similar approach by Panagiotidis et al. (2017), the R^2 value was about 0.75 in plot 1 and the mean absolute error was 2.62. Furthermore, Lim Ye et al. (2015) applied the differences of individual tree estimations from drone and ground truth data. The range was from 0 to 2 with root mean square error is 1.51. They used world view 3, UAV multispectral imagery, and terrestrial data to validate. The R^2 was less than 1 compared to each method used. According to He et al. (2019) height estimation from mountainous terrain contained an R^2 value of 0.83 respectively.

Compare to previous studied of extracting tree height from CHM, our result contained a lower accuracy which was caused by several factors (Table 10 and Figure 20):

- The designed GCPs were not fully applied to aligned images. They were used for geo-referencing.
- The pipe high were shorter as professional equipment for height measurement. Moreover, the measurement higher than 5 m was caused misleading results.
- Cashew tree crowns are not easy to see the treetop due to the complex leaves.
- The equipment used to measure was not high grade, the accuracy was less than 0.5 m. Measurement under tree and its limitation has been discussed(Bastos & Hasegawa, 2013; Morales & Tsubouchi, 2007; Næsset & Jonmeister, 2002; Sawaguchi, Nishida, Shishiuchi, & Tatsukawa, 2003)
- Tree locations were based on stand of tree while some the cashew tree did not stand straight
- Clouds affect the obtained images in at approx. 50 %, therefore, an auto aperture, with shutter speed and iso were used.
- The differentiation of small vegetation from the ground caused difficulties.
- Semi-automatic point cloud classification did not well classify during high flight attribute with low point cloud densities.
- Resampling methods were not affected to the result of photogrammetric software. Previous studies have not yet mentioned about resample results from photogrammetric software
- An example of bias from orthophoto T028, field measurement was less than the estimated 1.7 m which may caused by the provided the tree location. Tree location and height were measured at the same time based on a single point. In contrast, the extraction method, zonal statistics, calculated the highest point, maximum, of pixel values while it was based on tree stump. In contrast, T040 was field measurement larger than the estimated 2 m. The orthophoto were indicated that the buffering goes to non-vegetation. This caused a calculation of the highest values of none ground with ground and the result.
- Systematic errors from image smoothing may to produce results with low accuracy.

The result of this study is may contain an acceptable accuracy due to the equipment applied. The outcome of the research is enough for the purpose of it. It was shown that the used method can be used for forest monitoring variation respectively to forest management (Panagiotidis et al., 2017).

CHAPTER 5
CONCLUSION AND RECOMMENDATION

5.1 Conclusion

5.1.1 Considering with difference flight attributes, is there any difference of height estimation upon the altitude?

In our experiments, the flight used the same settings. The bias was less than 1 m with mean absolute error less than 1 m from point cloud classification. Extreme bias were observed with photogrammetry products due to the bias larger than 1 m with mean absolute error range from 0.5 m to 4.4 m. Based on point cloud classification, the 50 m flight produced better results than the 200m flight. Processing of the data with photogrammetry products delivered inacceptable results for the 50 m flight with high bias. We can conclude that cashew height estimation from 50 m flight were good for the generation of tree heights from CHM in terms of point cloud classification. On the other hand, the generation of cashew tree height from photogrammetry products, 200 m flight provided better results compared to ground data.

5.1.2 How to choose correct flight attributes for tree height estimation?

In our experiment, the flight attribute depends on the target and the size of the project. The 50 m and the 200 m flight produced similar results. The use of GCPs in order to improve the accuracy of images, the 50 m flight allowed a selection. A marking of GCPs during the 200 m flight were complicated to select the center of GCPs even with a size of 1.5 m x 1.5 m. However, the used UAVs had a maximum speed at 3.9 m/s for the 50 m flight. The large area took a very long time to capture, approx. 1ha/5minutes. At an altitude of 200 m the flight velocity could be increased, however to be able to compare the results it was rejected.

5.1.3 How does the accuracy of photogrammetry product performance in tree height estimation?

According to our experiment, the photogrammetry product applied to generate CHM were acceptable with 200 m while applying default settings with geo-referenced (B011). The 200 m flight with default settings used geo-referenced or no geo-referenced (B017, B018, and B019). The results R^2 show that B011 was 0.41, B017 was 0.41, B018 was 0.43, B019 was 0.40. The product from 50 m flight all settings were low accuracy with R^2 values of less than 0.2. The photogrammetry results from

200 m flight were comparable with 50 m flight, the t-test indicated no statistically significant difference.

5.1.4 Extraction tree height from Canopy Height Model (CHM), which extraction methods (none-buffering and buffering) provide better accuracy?

The experiment with 5 different buffers, no buffer, 50 cm buffer, 100 cm buffer, 150 cm buffer, and 200 cm buffer showed for extraction of the 50 m flight different results, without buffer it was 0.83, with a 50 cm buffer was 0.33, with a 100 m buffer was 0.10, with a 150 m buffer was 0.03 and with a 200 m buffer was 0.15. The extraction in 200 m flight without buffer was 1.37, with a 50 cm buffer was 0.96, with a 100m buffer was 0.64, with a 150 m buffer was 0.44 and with a 20 0cm buffer was 0.28. We can conclude that 150 cm buffer are suitable for 50 m flights and 200 cm buffer are suitable for 200 m flights.

5.1.5 How does the accuracy of field measurement validate the tree estimated?

In our research, even though we used designed pipe meters to measure tree height. We were able to derive tree heights comparable with estimated results. The linear regression provided a medium relationship of R^2 in the range of 0.40 to 0.60. In a comparison between ground data and estimates, there are no statically significant differences between buffers of 100 cm, 150 cm and 200 cm. We can conclude that our field data are acceptable with 50m flight using semi-automatic point cloud classification.

The focus of this study was to estimate the tree heights of cashew trees at Kulen Mountain using low-cost UAV. We generated CHM from our UAV images. Our results showed that we got lower accuracy compared to previous studies which is due to our images quality and some limitations from our equipment and techniques. The proposed method are possible for open terrains with less than 12 m as we used not professional equipment and cashew tree have complex leaves. Therefore, we had some issues in order to identify treetops. Furthermore, GCPs collected were not helpful due to the block of canopy. Regarding the performances of tree height estimation from UAV versus field measured, we can assume that the workflow of UAV is faster and effectively compared to field measurements which is time and resources consuming.

5.2 Recommendation

In our experiment, there are can be done some improvements in order to increase accuracy as most questions were not yet answered clearly. Especially the estimation of cashew tree height estimation using low-UAV is still tricky as it was the first experiment in Cambodia. In order to improve future experiment, some recommendations:

- Comparison of various remote sensing applications use to derive high accuracy of height estimation from cashew trees
- CHM model will be better to generate tree height estimation. If difference photogrammetry techniques are considerable due to the limitation of the positioning of images or image matching. In our research, accuracy of field measurement GCPs, tree height, and tree positions were challenging which need more improvement.
- The photogrammetry method to generate DTM and DSM without applying smooth filtering and shape on surface. In our experiment, the smooth filtering and shape may affect the DTM automatic classification which lead almost all photogrammetry products got low accuracy.
- Airsoft metaphase is another photogrammetry software, it is also good and may solve some limitations of our low accuracy.
- In our works, we don't use real time kinematic (RTK) from drone due to our DJI Phantom 4 RTK as it was not available. It collects data with real time which may provide better faster and more accurate data. It would enable the work in large scales.
- Different flight altitudes from 50 m to 500 m could be tested. Additional testing with different overlaps. The speed of flight should be considered due to the size of future projects
- Crown cover overlapping is hard to define. Measuring the tree height by extraction from CHM shall be considered with crown area.

The buffering method should consider with tree crown and explore the underestimate or overestimate by using orthophoto overlap with buffer zone.

REFERENCES

Andreo, V. (2013). *Remote Sensing and Geographic Information Systems in Precision Farming*.

Anthony, D., Elbaum, S., Lorenz, A., & Detweiler, C. (2014, 14-18 Sept. 2014). *On crop height estimation with UAVs.* Paper presented at the 2014 IEEE/RSJ International Conference on Intelligent Robots and Systems.

Awange, J., & Kiema, J. (2019). Fundamentals of Photogrammetry. In J. Awange & J. Kiema (Eds.), *Environmental Geoinformatics: Extreme Hydro-Climatic and Food Security Challenges: Exploiting the Big Data* (pp. 161-178). Cham: Springer International Publishing.

Bastos, A. S., & Hasegawa, H. (2013). Behavior of GPS Signal Interruption Probability under Tree Canopies in Different Forest Conditions. *European Journal of Remote Sensing, 46*(1), 613-622. doi:10.5721/EuJRS20134636

Becker, C., Rosinskaya, E., Häni, N., d'Angelo, E., & Strecha, C. (2018). Classification of Aerial Photogrammetric 3D Point Clouds. *Photogrammetric Engineering and Remote Sensing, 84*, 287-295. doi:10.14358/PERS.84.5.287

Berie, H. T., & Burud, I. (2018). Application of unmanned aerial vehicles in earth resources monitoring: focus on evaluating potentials for forest monitoring in Ethiopia. *European Journal of Remote Sensing, 51*(1), 326-335. doi:10.1080/22797254.2018.1432993

Birdal, A. (2016). *Determination of Tree Heights With Unmanned Air Vehicles.*

Birdal, A. C., Avdan, U., & Türk, T. (2017). Estimating tree heights with images from an unmanned aerial vehicle. *Geomatics, Natural Hazards and Risk, 8*(2), 1144-1156. doi:10.1080/19475705.2017.1300608

Bragg, D. (2014). Accurately Measuring the Height of (Real) Forest Trees. *Journal of Forestry -Washington-, 112*, 51-54. doi:10.5849/jof.13-065

Cambodia, M. o. E. (2017). *Management Programme Kulen Mountain National Park 2018-2027*. Retrieved from http://www.cambodia-redd.org/wp-content/uploads/2017/10/Kulen-Strategy%E2%80%8B%E2%80%8B%E2%80%8B-English-resized.pdf.

Chan, E., Fung, T., & Wong, F. (2021). Estimating above-ground biomass of subtropical forest using airborne LiDAR in Hong Kong. *Scientific Reports, 11*. doi:10.1038/s41598-021-81267-8

CHCNAV. (2018). CHC E91 GNSS Receiver user guide. Retrieved from https://fccid.io/SY4-A01013/User-Manual/User-Manual-4095571

Daley, N., Burnett, C., Wulder, M., Niemann, K., & Goodenough, D. (1999). Comparison of Fixed-size and Variable-sized Windows for the Estimation of Tree Crown Position.

Díaz-Varela, R. A., De la Rosa, R., León, L., & Zarco-Tejada, P. J. (2015). High-Resolution Airborne UAV Imagery to Assess Olive Tree Crown Parameters Using 3D Photo Reconstruction: Application in Breeding Trials. *Remote Sensing, 7*(4). doi:10.3390/rs70404213

Dobbertin, M., Neumann, M., & Schroeck, H.-W. (2013). Chapter 10 - Tree Growth Measurements in Long-Term Forest Monitoring in Europe. In M. Ferretti & R. Fischer (Eds.), *Developments in Environmental Science* (Vol. 12, pp. 183-204): Elsevier.

Emlid. (2019). Single-band RTK GNSS receiver with centimeter precision. Retrieved from https://emlid.com/reachrs/

Engineering, C. O. (2015). *Procedures for Processing LIDAR Point Cloud Files to Create Digital Elevation Models, Contours, and Elevation Changes*. Retrieved from

Fernandez-Diaz, J., Singhania, A., Caceres, J., Slatton, K., Starek, M., Kumar, R., & Slatton, P. (2008). An overview of lidar point cloud processing software.

Ganz, S., Käber, Y., & Adler, P. (2019). Measuring Tree Height with Remote Sensing—A Comparison of Photogrammetric and LiDAR Data with Different Field Measurements. *Forests, 10*(8). doi:10.3390/f10080694

Girardeau-Montaut, D. (2016). CloudCompare. *Retrieved from CloudCompare: https://www. danielgm. net/cc*.

Graham, L. (2012). The LAS 1.4 specification. *Photogrammetric Engineering and Remote Sensing, 78*(2), 93-102.

Guerra, J., González-Ferreiro, E., Sarmento, A., Silva, J., Nunes, A., Correia, A., . . . Díaz Varela, R. (2016). Using high resolution UAV imagery to estimate tree variables in Pinus pinea plantation in Portugal. *Forest Systems, 25*, eSC09. doi:10.5424/fs/2016252-08895

Harmon, M. (2011). *t-tests in Excel-The Excel statistical master*: Mark Harmon.

Hartley, R., Leonardo, E., Massam, P., Watt, M., Estarija, H., Wright, L., . . . Pearse, G. (2020). An Assessment of High-Density UAV Point Clouds for the Measurement of Young Forestry Trials. *Remote Sensing, 12*, 4039. doi:10.3390/rs12244039

He, H., Yan, Y., Chen, T., & Cheng, P. (2019). Tree Height Estimation of Forest Plantation in Mountainous Terrain from Bare-Earth Points Using a DoG-Coupled Radial Basis Function Neural Network. *Remote Sensing, 11*, 1271. doi:10.3390/rs11111271

Hentz, Â. M. K., Dalla Corte, A. P., Netto, S. P., Strager, M. P., & Schoeninger, E. R. (2018). Treedetection: Automatic tree detection using UAV-based data. *Floresta, 48*(3), 393-402.

Islami, M. M., Rusolono, T., Setiawan, Y., Rahadian, A., Hudjimartsu, S. A., & Prasetyo, L. B. (2021). HEIGHT, DIAMETER AND TREE CANOPY COVER ESTIMATION BASED ON UNMANNED AERIAL VEHICLE (UAV) IMAGERY WITH VARIOUS ACQUISITION HEIGHT. *Media Konservasi, 26*(1), 17-27.

Ivosevic, B., Han, Y.-G., & Kwon, O. (2017). Calculating coniferous tree coverage using unmanned aerial vehicle photogrammetry. *Journal of Ecology and Environment, 41*(1), 10. doi:10.1186/s41610-017-0029-0

Jackson, J., Saborio, R., Ghazanfar, S. A., Gebre-Egziabher, D., & Davis, B. (2018). Evaluation of low-cost, centimeter-level accuracy OEM GNSS receivers.

Jin, C., Oh, C.-y., Shin, S., Njungwi, N., & Choi, C. (2020). A Comparative Study to Evaluate Accuracy on Canopy Height and Density Using UAV, ALS, and Fieldwork. *Forests, 11*, 241. doi:10.3390/f11020241

Jurjević, L., Liang, X., Gašparović, M., & Balenović, I. (2020). Is field-measured tree height as reliable as believed – Part II, A comparison study of tree height estimates from conventional field measurement and low-cost close-range remote sensing in a deciduous forest. *ISPRS Journal of Photogrammetry and*

Remote Sensing, 169, 227-241.
doi:https://doi.org/10.1016/j.isprsjprs.2020.09.014

Kameyama, S., & Sugiura, K. (2020). Estimating Tree Height and Volume Using Unmanned Aerial Vehicle Photography and SfM Technology, with Verification of Result Accuracy. *Drones, 4*(2), 19.

Krause, S., Sanders, T., Mund, J.-P., & Greve, K. (2019a). UAV-Based Photogrammetric Tree Height Measurement for Intensive Forest Monitoring. *Remote Sensing, 11*, 758. doi:10.3390/rs11070758

Krause, S., Sanders, T. G. M., Mund, J.-P., & Greve, K. (2019b). UAV-Based Photogrammetric Tree Height Measurement for Intensive Forest Monitoring. *Remote Sensing, 11*(7). doi:10.3390/rs11070758

Lague, D., Brodu, N., & Leroux, J. (2013). Accurate 3D comparison of complex topography with terrestrial laser scanner: Application to the Rangitikei canyon (N-Z). *ISPRS Journal of Photogrammetry and Remote Sensing, 82*, 10-26. doi:https://doi.org/10.1016/j.isprsjprs.2013.04.009

Larjavaara, M., & Muller-Landau, H. C. (2013). Measuring tree height: a quantitative comparison of two common field methods in a moist tropical forest. *Methods in Ecology and Evolution, 4*(9), 793-801. doi:https://doi.org/10.1111/2041-210X.12071

Larjavaara, M., & Muller-Landau, H. C. (2013). Measuring tree height: a quantitative comparison of two common field methods in a moist tropical forest. *Methods in Ecology and Evolution, 4*(9), 793-801.

Li, L., Chen, J., Mu, X., Li, W., Yan, G., Xie, D., & Zhang, W. (2020). Quantifying Understory and Overstory Vegetation Cover Using UAV-Based RGB Imagery in Forest Plantation. *Remote Sensing, 12*, 298. doi:10.3390/rs12020298

Li, Y.-Q., Deng, X., Huang, Z.-H., Xiang, W., Yan, W.-d., Lei, P., . . . Peng, C.-H. (2015). Development and Evaluation of Models for the Relationship between Tree Height and Diameter at Breast Height for Chinese-Fir Plantations in Subtropical China. *PLOS ONE, 10*, e0125118. doi:10.1371/journal.pone.0125118

Liang, X., Kukko, A., Kaartinen, H., Hyyppä, J., Yu, X., Jaakkola, A., & Wang, Y. (2013). Possibilities of a Personal Laser Scanning System for Forest Mapping and Ecosystem Services. *Sensors (Basel, Switzerland), 14*, 1228-1248. doi:10.3390/s140101228

Lim Ye, S., La Phu, H., Park Jong, S., Lee Mi, H., Pyeon Mu, W., & Kim, J.-I. (2015). Calculation of Tree Height and Canopy Crown from Drone Images Using Segmentation. 한국측량학회지, *33*(6), 605-614. doi:10.7848/KSGPC.2015.33.6.605

Lussem, U., Schellberg, J., & Bareth, G. (2020). Monitoring Forage Mass with Low-Cost UAV Data: Case Study at the Rengen Grassland Experiment. *PFG – Journal of Photogrammetry Remote Sensing and Geoinformation Science, 88*. doi:10.1007/s41064-020-00117-w

Marcu, C. (2018). *Tree species classification in Romania using RapidEye and LiDAR data*.

Meghani, N., Miller, D., & Holderman, B. (2017). *ACCURACY OF SUAS OPERATIONS IN DENSELY FORESTED AREAS WITH USE OF EMLID REACH RTK SYSTEM*.

MILLIKAN, P. H. K., SILVA, C. A., Rodriguez, L. C. E., Oliveira, T. M. d., Carvalho, M. P. d. L. C. e., & Carvalho, S. d. P. C. e. (2019). AUTOMATED INDIVIDUAL TREE DETECTION IN AMAZON TROPICAL FOREST FROM AIRBORNE LASER SCANNING DATA. *CERNE, 25*, 273-282.

Moe, K. T., Owari, T., Furuya, N., & Hiroshima, T. (2020). Comparing Individual Tree Height Information Derived from Field Surveys, LiDAR and UAV-DAP for High-Value Timber Species in Northern Japan. *Forests, 11*(2). doi:10.3390/f11020223

Montealegre, A. L., Lamelas, M. T., & Riva, J. D. (2015). Interpolation Routines Assessment in ALS-Derived Digital Elevation Models for Forestry Applications. *Remote Sensing, 7*(7). doi:10.3390/rs70708631

Morales, Y., & Tsubouchi, T. (2007). *DGPS, RTK-GPS and StarFire DGPS performance under tree shading environments*.

Næsset, E., & Jonmeister, T. (2002). Assessing Point Accuracy of DGPS Under Forest Canopy Before Data Acquisition, in the Field and After Postprocessing. *Scandinavian Journal of Forest Research - SCAND J FOREST RES, 17*, 351-358. doi:10.1080/02827580260138099

Navarro, A., Young, M., Allan, B., Carnell, P., Macreadie, P., & Ierodiaconou, D. (2020). The application of Unmanned Aerial Vehicles (UAVs) to estimate above-ground biomass of mangrove ecosystems. *Remote Sensing of Environment, 242*, 111747. doi:https://doi.org/10.1016/j.rse.2020.111747

Ojoatre, S. (2016). *Accuracy of measuring tree height using Airborne LiDAR and Terrestrial laser scanner and its effect on estimating forest biomass and carbon stock in Ayer Hitam tropical rain forest reserve, Malaysia.* University of Twente,

Osińska-Skotak, K., Bakuła, K., Jełowicki, Ł., & Podkowa, A. (2019). Using Canopy Height Model Obtained with Dense Image Matching of Archival Photogrammetric Datasets in Area Analysis of Secondary Succession. *Remote Sensing, 11*, 2182. doi:10.3390/rs11182182

Panagiotidis, D., Abdollahnejad, A., Surovy, P., & Chiteculo, V. (2017). Determining tree height and crown diameter from high-resolution UAV imagery. *International Journal of Remote Sensing, 38*. doi:10.1080/01431161.2016.1264028

Paneque-Gálvez, J., McCall, M. K., Napoletano, B. M., Wich, S. A., & Koh, L. P. (2014). Small Drones for Community-Based Forest Monitoring: An Assessment of Their Feasibility and Potential in Tropical Areas. *Forests, 5*(6). doi:10.3390/f5061481

Peng, X., Zhao, A., Chen, Y., Chen, Q., & Liu, H. (2021). Tree Height Measurements in Degraded Tropical Forests Based on UAV-LiDAR Data of Different Point Cloud Densities: A Case Study on Dacrydium pierrei in China. *Forests, 12*(3). doi:10.3390/f12030328

Phalla, T., Ota, T., Mizoue, N., Kajisa, T., Yoshida, S., Vuthy, M., & Sokh, H. (2018). The Importance of Tree Height in Estimating Individual Tree Biomass while Considering Errors in Measurements and Allometric Models. *Agrivita, 40*, 131-140. doi:10.17503/agrivita.v40i1.1730

Pix4D. (November 5, 2018). Do more GCPs equal more accurate drone maps? Retrieved from https://www.pix4d.com/blog/GCP-accuracy-drone-maps

Popescu, S. C., Wynne, R. H., & Nelson, R. F. (2002). Estimating plot-level tree heights with lidar: local filtering with a canopy-height based variable window size. *Computers and Electronics in Agriculture, 37*(1), 71-95. doi:https://doi.org/10.1016/S0168-1699(02)00121-7

Prisacariu, V. (2017). The history and the evolution of UAVs from the beginning till the 70s. *Journal of Defense Resources Management (JoDRM), 8*(1), 181-189.

Ramli, M., & Tahar, K. N. (2020). Homogeneous tree height derivation from tree crown delineation using Seeded Region Growing (SRG) segmentation. *Geo-spatial Information Science, 23*, 1-14. doi:10.1080/10095020.2020.1805366

Ramli, M. F., & Tahar, K. N. (2020). Homogeneous tree height derivation from tree crown delineation using Seeded Region Growing (SRG) segmentation. *Geo-spatial Information Science, 23*(3), 195-208. doi:10.1080/10095020.2020.1805366

Romero-Toro-Gascueña, I., Sastre-Merino, S., Guillén, J., Ayuga-Téllez, E., Garcia-Garcia, M., González-García, C., & Grande-Ortíz, M. (2011). Comparison of Interpolation Methods for the Study of Forest Variables Using a Geographic Information System. *Journal of Agricultural Science and Technology, 1*, 428-436.

Ross, S. M. (2014). Chapter 2 - Descriptive Statistics. In S. M. Ross (Ed.), *Introduction to Probability and Statistics for Engineers and Scientists (Fifth Edition)* (pp. 9-51). Boston: Academic Press.

Sawaguchi, I., Nishida, K., Shishiuchi, M., & Tatsukawa, S. (2003). Positioning precision and sampling number of DGPS under forest canopies. *Journal of Forest Research, 8*(2), 0133-0137. doi:10.1007/s103100300017

Sibona, E., Vitali, A., Meloni, F., Caffo, L., Dotta, A., Lingua, E., . . . Garbarino, M. (2017). Direct Measurement of Tree Height Provides Different Results on the Assessment of LiDAR Accuracy. *Forests, 8*(1). doi:10.3390/f8010007

SILVA, C. A., KLAUBERG, C., HUDAK, A. T., VIERLING, L. A., LIESENBERG, V., BERNETT, L. G., . . . SCHOENINGER, E. R. (2018). Estimating Stand Height and Tree Density in Pinus taeda plantations using in-situ data, airborne LiDAR and k-Nearest Neighbor Imputation. *Anais da Academia Brasileira de Ciências, 90*, 295-309.

Singh, M., Evans, D., Chevance, J.-B., Boun, Tan, S., Wiggins, N., . . . Sakhoeun, S. (2018). Evaluating the ability of community-protected forests in Cambodia to prevent deforestation and degradation using temporal remote sensing data. *Ecology and Evolution, 8*, 1-17. doi:10.1002/ece3.4492

Singh, M., Evans, D., Chevance, J.-B., Tan, B., Wiggins, N., Kong, L., & Sakhoeun, S. (2019). Evaluating remote sensing datasets and machine learning algorithms for mapping plantations and successional forests in Phnom Kulen National Park of Cambodia. *PeerJ, 7*, e7841. doi:10.7717/peerj.7841

Singh, M., Evans, D., Tan, B. S., & Nin, C. S. (2015). Mapping and Characterizing Selected Canopy Tree Species at the Angkor World Heritage Site in Cambodia Using Aerial Data. *PLOS ONE, 10*(4), e0121558. doi:10.1371/journal.pone.0121558

Singhal, G., Bansod, B., & Mathew, L. (2018). *Unmanned Aerial Vehicle Classification, Applications and Challenges: A Review*.

Skovsgaard, J. P. (2004). MENSURATION | Forest Measurements. In J. Burley (Ed.), *Encyclopedia of Forest Sciences* (pp. 550-566). Oxford: Elsevier.

St-Onge, B., Treitz, P., & Wulder, M. (2003). Tree and Canopy Height Estimation with Scanning Lidar. *Remote sensing of forest environments: concepts and case studies*, 489-509. doi:10.1007/978-1-4615-0306-4_19

Su, W., Liu, R., Liu, T., Huang, J., Zhang, X., & Liu, J. (2012). *The Estimation of Tree Height Based on LiDAR Data and QuickBird Imagery*.

Taddia, Y., Stecchi, F., & Pellegrinelli, A. (2020). Coastal Mapping using DJI Phantom 4 RTK in Post-Processing Kinematic Mode. *Drones, 4*, 9. doi:10.3390/drones4020009

Tian, J., Dai, T., Li, H., Liao, C., Teng, W., Hu, Q., . . . Xu, Y. (2019). A Novel Tree Height Extraction Approach for Individual Trees by Combining TLS and UAV Image-Based Point Cloud Integration. *Forests, 10*, 537. doi:10.3390/f10070537

Tong, G., Li, Y., Dong, C., Sun, Q., Cao, W., & Xiang, G. (2020). CSPC-Dataset: New LiDAR Point Cloud Dataset and Benchmark for Large-scale Semantic Segmentation. *IEEE Access, PP*, 1-1. doi:10.1109/ACCESS.2020.2992612

Traore, S. O. (2021). *Abstract (UAV)*.

Van Laar, A., & Akça, A. (2007). *Forest mensuration* (Vol. 13): Springer Science & Business Media.

West, P. (2009). *Tree and forest measurement: 2nd edition*.

Wong, W. V. C., & Tsuyuki, S. (2017). Chapter 7 - High Resolution of Three-Dimensional Dataset for Aboveground Biomass Estimation in Tropical Rainforests. In G. P. Shivakoti, U. Pradhan, & Helmi (Eds.), *Redefining Diversity & Dynamics of Natural Resources Management in Asia, Volume 1* (pp. 115-130): Elsevier.

Wu, D., Johansen, K., Phinn, S., Robson, A., & Tu, Y.-H. (2020). Inter-comparison of remote sensing platforms for height estimation of mango and avocado tree crowns. *International Journal of Applied Earth Observation and Geoinformation, 89*, 102091. doi:https://doi.org/10.1016/j.jag.2020.102091

Wulder, M., Niemann, K., & Goodenough, D. (2000). Local Maximum Filtering for the Extraction of Tree Locations and Basal Area from High Spatial Resolution Imagery. *Remote Sensing of Environment, 73*, 103-114. doi:10.1016/S0034-4257(00)00101-2

Yastikli, N., & Cetin, Z. (2016). CLASSIFICATION OF LiDAR DATA WITH POINT BASED CLASSIFICATION METHODS. *ISPRS - International Archives of the Photogrammetry, Remote Sensing and Spatial Information Sciences, XLI-B3*, 441-445. doi:10.5194/isprs-archives-XLI-B3-441-2016

Zainuddin, K., Jaffri, M., Zainal, M. Z., Ghazali, N., & Samad, A. M. (2016). *Verification test on ability to use low-cost UAV for quantifying tree height*.

Zarco-Tejada, P., Díaz Varela, R., Angileri, V., & Loudjani, P. (2014). Tree height quantification using very high resolution imagery acquired from an unmanned aerial vehicle (UAV) and automatic 3D photo-reconstruction methods. *European Journal of Agronomy, 55*, 89–99. doi:10.1016/j.eja.2014.01.004

Zhang, W., Qi, J., Peng, W., Wang, H., Xie, D., Wang, X., & Yan, G. (2016). An Easy-to-Use Airborne LiDAR Data Filtering Method Based on Cloth Simulation. *Remote Sensing, 8*, 501. doi:10.3390/rs8060501

Zhou, X., Wang, W., Di, L., Lu, L., & Guo, L. (2020). Estimation of Tree Height by Combining Low Density Airborne LiDAR Data and Images Using the 3D Tree Model: A Case Study in a Subtropical Forest in China. *Forests, 11*(12). doi:10.3390/f11121252

BIOGRAPHY

NAME	Ly Mot
DATE OF BIRTH	07 August 2565
PLACE OF BIRTH	Cambodia
PRESENT ADDRESS	St2002, Tuek Tla, Phnom Penh Tmey, Sen Sok, Phnom Penh
EDUCATION	2019 – 2021 M.Eng. in Photogrammetry and Remote Sensing, LIEMARS, Wuhan University (WHU), China. 2019 – 2021 M.Sc in Remote sensing and GIS Burapha University (BUU), Thailand 2015 – 2019 B.Sc in Environmental Science at Royal University of Phnom Penh (RUPP), Cambodia
AWARDS OR GRANTS	2020, Best Paper Award "Visualization Analysis of COVID-19 to Respond to Infectious Disease Outbreaks Using Geoinformatics Techniques in Thailand: Opportunities and Challenges", The 7th International Conference on Health GIS 2020 2019, SCGI Masters Program Scholarship. Funded by GISTDA Ministry of Higher Education, Science, Research and Innovation of Thailand.